Modeling and Simulation of Piezocomposites

Jacob Fish and Wen Chen

Department of Mechanical, Aerospace and Nuclear Engineering

Rensselaer Polytechnic Institute, Troy, NY 12180, USA

Abstract: Solution procedures for large-scale transient analysis of piezocomposites are developed. Computational efficiency of unconditionally stable and conditionally stable implicit partitioned schemes as well as explicit partitioned schemes is investigated in the context of multilevel solution methods applied to separate field equations.

1.0 Introduction

Multiphysics modeling and simulation has recently gained significant attention in computational science and engineering community. Example problems falling into this category are coupled mechanical, thermal, electrical, diffusion-reaction, fluid-structure interaction problems. In multiphysics problems, typically a wide range of interacting spatial and temporal scales are involved resulting in large coupled time-dependent system of equations.

Generally, there are three approaches for simulation of coupled systems [1]: field elimination, monolithic and partitioned schemes. Field elimination is restricted to linear (or linearized) problems that permit efficient decoupling. The monolithic scheme is in general computationally challenging, economically suboptimal and software-wise unmanageable [2]. On the other hand, the partitioned treatment, which is the focus of the present manuscript, is computational efficient, flexible and software reusable.

In partitioned schemes, computational efficiency is counteracted by the fact that satisfactory numerical stability is hard to achieve. In fact the practical feasibility of the partitioned approach hinges entirely on the stability analysis [1]. Stability analysis by standard Fourier techniques using a scalar test equation is not generally possible because modes of individual subsystems are not modes of the coupled problem. Moreover, partitioned procedures are in general less accurate than their underlying subsystem time integrators. In principle, higher order accuracy can be recovered by iterating the solution between the fields at each time step [3]. However, the computational cost of interfield iterations may overshadow the gains from reduced timesteping [1].

In this manuscript we focus on the problem of piezoelectricity in periodic heterogeneous media. We start by formulating the monolithic equations and study stability of implicit time integrators (the Newmark method) applied to the monolithic equations. It is demonstrated that taking the integration parameters which render the Newmark method unconditionally stable for conventional structural dynamics problems do not guarantee unconditional stability of the monolithic system. This is due to the fact that in structural dynamics problems, the global mass matrix is positive definite and the stiffness matrix is at least positive semi-definite, whereas for piezocomposites the global stiffness matrix of the monolithic scheme is indefinite, and thus conventional implicit integrators directly

applied to the monolithic system may not be stable. From the monolithic equations, we construct the implicit partitioned schemes based on the block Gauss-Seidel method. It is shown that the partitioned scheme constructed directly from the monolithic equations does not guarantee unconditional stability. Unconditionally stable partitioned scheme can be obtained by augmenting the original equations of motion and subsequently splitting the field equations along the lines of block Gauss-Seidel method.

Computational efficiency of solving the problem of piezoelectricity is the main focus of the present manuscript. While partitioned approach reduces the solution of coupled physics problem into a sequence of single field problems, the computational cost could be still insurmountable due to the existence of multiple spatial scales within each physical process. For this type of problems the direct method may not computationally optimal, while various multigrid methods though very efficient for differential equations with constant coefficients, exhibit poor rates of convergence when applied to differential equations with rapidly oscillating coefficients [4][5]. The Representative Volume Element or RVE-based multilevel method developed by the authors has been shown to possess high rates of convergence for single-field structural dynamics problems in periodic heterogeneous media [6]. In the present manuscript, we extend the framework of the RVE-based multilevel method to transient analysis of piezocomposites.

Convergence properties of the RVE-based multilevel method are studied in the context of unconditionally stable and a conditionally stable implicit and explicit partitioned schemes. We show that the rate of convergence of the RVE-based multilevel method for conditionally stable implicit and explicit partitioned schemes is higher than for unconditionally stable scheme. This is in part due to the fact that the eigenspace of the stabilized matrix cannot be reproduced by a linear combination of the Representative Volume Elements. For high frequency applications, the conditionally stable implicit and explicit partitioned schemes are advantageous, since the choice of time step is governed by accuracy considerations, whereas the unconditionally stable schemes might be better suited for low frequency applications.

2.0 Finite Element Formulation of Piezoelectricity

2.1 Governing equations of piezoelectricity

Let Ω denote the domain of interest, and Γ the boundary of Ω. Consider the governing equations of linear piezoelectricity, which include:

i. Mechanical equilibrium

$$\sigma_{ij,j} + f_i = \rho \ddot{u}_i \tag{1}$$

ii. Maxwell's equation of equilibrium (assumed to be quasi-static and decoupled from mechanical fields)

$$D_{i,i} = 0 \tag{2}$$

iii. Constitutive equations

$$\sigma_{ij} = C_{ijkl}S_{kl} - e_{kij}E_k, \qquad D_i = e_{ikl}S_{kl} + \varepsilon_{ik}E_k \tag{3}$$

iv. Strain-displacement relation and the curl-free electric field

$$S_{ij} = \frac{1}{2}(u_{i,j} + u_{j,i}), \qquad E_i = -\phi_{,i} \tag{4}$$

where σ, $\boldsymbol{S}$, $\boldsymbol{E}$ and $\boldsymbol{D}$ are the stress, strain, electric field and electric displacement vectors, respectively; $\boldsymbol{C}$, ε, and $\boldsymbol{e}$ are the elastic tensor at constant electric field, dielectric tensor at constant strain field and the piezoelectric tensor, respectively; $\boldsymbol{u}$ and ϕ denote the displacement vector and electric potential (voltage), respectively; ρ is the mass density and $\boldsymbol{f}$ the body force. The superposed dot and comma denote temporal and spatial differentiation, respectively. Since the piezoelectric field $\boldsymbol{e}$ is a third-rank tensor, piezoelectric coupling exists in intrinsically anisotropic materials only [7].

To complete the description of the problem, the boundary conditions are prescribed as

$$u_i = \bar{u}_i \text{ on } \Gamma_u \quad \text{and} \quad \phi = \bar{\phi} \text{ on } \Gamma_\phi \tag{5}$$

$$\sigma_{ij}n_j = \bar{T}_i \text{ on } \Gamma_\sigma \quad \text{and} \quad D_i n_i = \bar{q} \text{ on } \Gamma_q \tag{6}$$

$$\Gamma_u \cup \Gamma_\sigma = \Gamma, \quad \Gamma_u \cap \Gamma_\sigma = 0; \qquad \Gamma_\phi \cup \Gamma_q = \Gamma, \quad \Gamma_\phi \cap \Gamma_q = 0 \tag{7}$$

where $\bar{\boldsymbol{u}}$ and $\bar{\boldsymbol{T}}$ are the prescribed mechanical displacement and surface traction, respectively; $\bar{\phi}$ and $\bar{q}$ are the prescribed electric potential and surface charge, respectively; $\boldsymbol{n}$ denotes the outward unit normal vector.

2.2 The weak formulation and semi-discrete equations of motion

From the governing equations (1) - (4) and boundary conditions (5) - (7), we establish the weak formulation of the problem

For $t \in (0, T]$, find $u_i(\boldsymbol{x}, t) \in V_m^{\bar{u}}$ and $\phi(\boldsymbol{x}) \in V_e^{\bar{\phi}}$, such that

$$\int_\Omega [\rho\ddot{u}_i - (\sigma_{ij,j} + f_i)]w_i d\Omega = 0 \qquad \forall w_i \in V_m^0 \tag{8}$$

$$\int_\Omega D_{i,i}\Psi d\Omega = 0 \qquad \forall \Psi \in V_e^0 \tag{9}$$

where

$$V_m^{\bar{u}} = \{\boldsymbol{w}(\boldsymbol{x}) \in H^1(\Omega), \boldsymbol{w} = \bar{\boldsymbol{u}} \ \ on \ \ \Gamma_u\} \tag{10}$$

$$V_e^{\bar{\phi}} = \{\phi(\boldsymbol{x}) \in H^1(\Omega), \phi = \bar{\phi} \ \ on \ \ \Gamma_\phi\} \tag{11}$$

$$V_m^0 = V_m^{\bar{u}}\Big|_{\bar{u}=0}, \qquad V_e^0 = V_e^{\bar{\phi}}\Big|_{\bar{\phi}=0} \tag{12}$$

$$H^1(\Omega) = \{\boldsymbol{w} = \boldsymbol{w}(\boldsymbol{x}), \boldsymbol{x} \in \Omega \,|\, \boldsymbol{w}, \nabla w_i \in L^2(\Omega)\} \tag{13}$$

with $L^2(\Omega)$ denoting the set of square-integrable functions over Ω.

Integrating Eqns (8) and (9) by parts and substituting the constitutive relations (3), the kinematics relation (4) and the natural boundary conditions (6) into the resulting equations, and exploiting the symmetry of the elastic tensor, we have

$$\int_\Omega \rho w_i \ddot{u}_i d\Omega + \int_\Omega S_{ij}(\boldsymbol{w})[C_{ijkl}S_{kl}(\boldsymbol{u}) + e_{kij}\phi_{,k}]d\Omega = \int_\Omega f_i w_i d\Omega + \int_{\Gamma_\sigma} \bar{T}_i w_i ds \tag{14}$$

$$\int_\Omega \Psi_{,i}[e_{ikl}S_{kl}(\boldsymbol{u}) - \varepsilon_{ik}\phi_{,k}]d\Omega = \int_{\Gamma_q} \bar{q}\Psi ds \tag{15}$$

where $\boldsymbol{S}(\boldsymbol{w}) = \nabla^s \boldsymbol{w}$ is the symmetric gradient of $\boldsymbol{w}$.

Subsequently the matrix notation is adopted. We employ finite element discretization with element shape functions denoted as $\boldsymbol{N_u}$ and $\boldsymbol{N}_\phi$

$$\boldsymbol{u} = \boldsymbol{N_u}\boldsymbol{U}^e, \qquad \phi = \boldsymbol{N}_\phi \Phi^e \tag{16}$$

where $\boldsymbol{U}^e$ and Φ^e are element nodal values. Differentiating Eqn (16) yields the element strain and electric field vectors

$$\boldsymbol{S} = \boldsymbol{B_u}\boldsymbol{U}^e, \qquad \boldsymbol{E} = -\nabla\phi = -\boldsymbol{B}_\phi \Phi^e \tag{17}$$

Inserting Eqns (16) and (17) into (14) and (15) we obtain the semi-discrete equations of motion of piezoelectricity

$$\boldsymbol{M_{uu}}\ddot{\boldsymbol{U}} + \boldsymbol{K_{uu}}\boldsymbol{U} + \boldsymbol{K_{u\phi}}\Phi = \bar{\boldsymbol{F}}, \qquad \boldsymbol{K_{\phi u}}\boldsymbol{U} - \boldsymbol{K_{\phi\phi}}\Phi = \bar{\boldsymbol{Q}} \tag{18}$$

where the assembly operators are defined in a usual manner:

$$\boldsymbol{M}_{\boldsymbol{uu}} = \mathop{\boldsymbol{A}}_{e=1}^{Ne} \int_{\Omega_e} \rho \boldsymbol{N}_{\boldsymbol{u}}^T \boldsymbol{N}_{\boldsymbol{u}} d\Omega_e \text{ .... consistent mass matrix}$$

$$\boldsymbol{K}_{\boldsymbol{uu}} = \mathop{\boldsymbol{A}}_{e=1}^{Ne} \int_{\Omega_e} \boldsymbol{B}_{\boldsymbol{u}}^T \boldsymbol{C} \boldsymbol{B}_{\boldsymbol{u}} d\Omega_e \text{ ... mechanical stiffness matrix}$$

$$\boldsymbol{K}_{\boldsymbol{u}\phi} = \mathop{\boldsymbol{A}}_{e=1}^{Ne} \int_{\Omega_e} \boldsymbol{B}_{\boldsymbol{u}}^T \boldsymbol{e}^T \boldsymbol{B}_{\phi} d\Omega_e, \; \boldsymbol{K}_{\phi\boldsymbol{u}} = \mathop{\boldsymbol{A}}_{e=1}^{Ne} \int_{\Omega_e} \boldsymbol{B}_{\phi}^T \boldsymbol{e} \boldsymbol{B}_{\boldsymbol{u}} d\Omega_e \text{ ...piezoelectric stiffness matrices}$$

$$\boldsymbol{K}_{\phi\phi} = \mathop{\boldsymbol{A}}_{e=1}^{Ne} \int_{\Omega_e} \boldsymbol{B}_{\phi}^T \varepsilon \boldsymbol{B}_{\phi} d\Omega_e \text{ ... dielectric stiffness matrix}$$

$$\bar{\boldsymbol{F}} = \mathop{\boldsymbol{A}}_{e=1}^{Ne} \int_{\Omega_e} \boldsymbol{N}_{\boldsymbol{u}}^T \boldsymbol{f} d\Omega_e + \mathop{\boldsymbol{A}}_{e=1}^{S_e^{\sigma}} \int_{\Gamma_{\sigma}^e} \boldsymbol{N}_{\boldsymbol{u}}^T \bar{\boldsymbol{T}} ds, \qquad \bar{\boldsymbol{Q}} = \mathop{\boldsymbol{A}}_{e=1}^{S_e^{q}} \int_{\Gamma_q^e} \boldsymbol{N}_{\phi}^T \bar{q} ds \text{ ... forcing vectors}$$

with Ne and S_e^{σ}, S_e^{q} denoting the total number of elements and the number of elements with prescribed boundary conditions, respectively.

3.0 Field Elimination and Monolithic Solution Schemes

3.1 Static condensation

Suitably grounding the structure by specifying one or more nodal values of the potential renders $\boldsymbol{K}_{\phi\phi}$ non-singular. From the second equation in (18), we have

$$\Phi = \boldsymbol{K}_{\phi\phi}^{-1} (\boldsymbol{K}_{\boldsymbol{u}\phi}^T \boldsymbol{U} - \bar{\boldsymbol{Q}}) \tag{19}$$

Substituting the above equation into the first equation in (18) yields

$$\boldsymbol{M}_{\boldsymbol{uu}} \ddot{\boldsymbol{U}} + \tilde{\boldsymbol{K}} \boldsymbol{U} = \tilde{\boldsymbol{F}} \tag{20}$$

where

$$\tilde{\boldsymbol{K}} = \boldsymbol{K}_{\boldsymbol{uu}} + \boldsymbol{K}_{\boldsymbol{u}\phi} \boldsymbol{K}_{\phi\phi}^{-1} \boldsymbol{K}_{\boldsymbol{u}\phi}^T, \qquad \tilde{\boldsymbol{F}} = \bar{\boldsymbol{F}} + \boldsymbol{K}_{\boldsymbol{u}\phi} \boldsymbol{K}_{\phi\phi}^{-1} \bar{\boldsymbol{Q}} \tag{21}$$

Equation (20) is obtained by field elimination or static condensation of the electric field. It can be observed that $\tilde{\boldsymbol{K}}$ and $\boldsymbol{M}_{\boldsymbol{uu}}$ are positive definite, and Eqn (20) can be easily solved by using either implicit or explicit time integrator. This approach has been adopted in [8][9]. While relatively easy to implement for small problems, static condensation suffers a number of drawbacks. First, the condensed stiffness matrix $\tilde{\boldsymbol{K}}$ is denser than $\boldsymbol{K}_{\boldsymbol{uu}}$, and second, it destroys spectral properties of $\boldsymbol{K}_{\boldsymbol{uu}}$, which could be taken advantage of in designing efficient multilevel iterative solvers.

3.2 Monolithic scheme

Exploiting symmetry, $\boldsymbol{K}_{\phi \boldsymbol{u}} = \boldsymbol{K}_{\boldsymbol{u}\phi}^{T}$, we can rearrange Eqn (18) in the monolithic form:

$$\boldsymbol{M}\ddot{\boldsymbol{d}} + \boldsymbol{K}\boldsymbol{d} = \boldsymbol{F} \tag{22}$$

where

$$\boldsymbol{M} = \begin{bmatrix} \boldsymbol{M}_{\boldsymbol{uu}} & \boldsymbol{0} \\ \boldsymbol{0} & \boldsymbol{0} \end{bmatrix}, \quad \boldsymbol{K} = \begin{bmatrix} \boldsymbol{K}_{\boldsymbol{uu}} & \boldsymbol{K}_{\boldsymbol{u}\phi} \\ \boldsymbol{K}_{\boldsymbol{u}\phi}^{T} & -\boldsymbol{K}_{\phi\phi} \end{bmatrix}, \quad \boldsymbol{d} = \begin{bmatrix} \boldsymbol{U} \\ \Phi \end{bmatrix}, \quad \boldsymbol{F} = \begin{bmatrix} \overline{\boldsymbol{F}} \\ \overline{\boldsymbol{Q}} \end{bmatrix} \tag{23}$$

It can be seen that $\boldsymbol{M}$ is positive semi-definite and $\boldsymbol{K}$ indefinite. The monolithic scheme for piezoelectricity has been adopted by a number of authors [10][11][12]. However, prior to applying time integration scheme with proven stability behavior to the monolithic equation (22) it is necessary to examine its suitability for problems of piezoelectricity. We focus on Newmark integrator

$$\boldsymbol{d}_{n+1} = \boldsymbol{d}_n + \Delta t \boldsymbol{v}_n + \Delta t^2 \left[\left(\frac{1}{2} - \beta \right) \boldsymbol{a}_n + \beta \boldsymbol{a}_{n+1} \right] \tag{24}$$

$$\boldsymbol{v}_{n+1} = \boldsymbol{v}_n + \Delta t [(1-\gamma)\boldsymbol{a}_n + \gamma \boldsymbol{a}_{n+1}] \tag{25}$$

where $\boldsymbol{d}_n$, $\boldsymbol{v}_n$ and $\boldsymbol{a}_n$ are the displacement, velocity and acceleration vectors at time t_n, respectively; Δt is the time step size; β and γ are parameters which determine the stability and accuracy of the Newmark method. For structural dynamics the Newmark scheme is unconditionally stable for $2\beta \geq \gamma \geq 1/2$.

The stability of the Newmark method can be investigated by using the energy method (cf. Hughes[13][14]). Equations (22) (with $\boldsymbol{F} = \boldsymbol{0}$), (24) and (25) can be combined to form the following identity:

$$\boldsymbol{a}_{n+1}^{T} \boldsymbol{B} \boldsymbol{a}_{n+1} + \boldsymbol{v}_{n+1}^{T} \boldsymbol{K} \boldsymbol{v}_{n+1} = \boldsymbol{a}_n^{T} \boldsymbol{B} \boldsymbol{a}_n + \boldsymbol{v}_n^{T} \boldsymbol{K} \boldsymbol{v}_n - (2\gamma - 1)[\boldsymbol{a}_n]^{T} \boldsymbol{B} [\boldsymbol{a}_n] \tag{26}$$

where

$$\boldsymbol{B} = \boldsymbol{M} + \Delta t^2\left(\beta - \frac{1}{2}\gamma\right)\boldsymbol{K}, \qquad [\boldsymbol{a}_n] = \boldsymbol{a}_{n+1} - \boldsymbol{a}_n \tag{27}$$

From the above two equations, it can be observed that if $\gamma \geq 1/2$ and $\boldsymbol{B}$ is positive definite, we have

$$\boldsymbol{a}_{n+1}^T \boldsymbol{B}\boldsymbol{a}_{n+1} + \boldsymbol{v}_{n+1}^T \boldsymbol{K}\boldsymbol{v}_{n+1} \leq \boldsymbol{a}_n^T \boldsymbol{B}\boldsymbol{a}_n + \boldsymbol{v}_n^T \boldsymbol{K}\boldsymbol{v}_n \tag{28}$$

which implies

$$\boldsymbol{a}_n^T \boldsymbol{B}\boldsymbol{a}_n + \boldsymbol{v}_n^T \boldsymbol{K}\boldsymbol{v}_n \leq \boldsymbol{a}_0^T \boldsymbol{B}\boldsymbol{a}_0 + \boldsymbol{v}_0^T \boldsymbol{K}\boldsymbol{v}_0, \qquad n = 1, 2, 3, \ldots \tag{29}$$

Therefore, $\boldsymbol{a}_n$ and $\boldsymbol{v}_n$ are bounded. If $\boldsymbol{K}$ is non-singular, from Eqn (22) (with $\boldsymbol{F} = \boldsymbol{0}$), we have $\|\boldsymbol{d}_n\| \leq \|\boldsymbol{K}^{-1}\| \|\boldsymbol{M}\| \|\boldsymbol{a}_n\|$, and then $\boldsymbol{d}_n$ is bounded. For $\boldsymbol{M}$ and $\boldsymbol{K}$ to be positive definite and at least positive semi-definite respectively, as is the case of elasto-dynamics, the matrix $\boldsymbol{B}$ is positive definite for $2\beta \geq \gamma$, which is the well-known condition for the Newmark scheme to be unconditionally stable. In the case of piezoelectricity $\boldsymbol{M}$ and $\boldsymbol{K}$ are positive semi-definite and indefinite, respectively, and thus the condition of $2\beta \geq \gamma$ does not guarantee positive-definiteness of $\boldsymbol{B}$. Nevertheless, in case of the average acceleration method (or trapezoidal rule) with $\beta = 1/4$ and $\gamma = 1/2$, the monolithic scheme applied to linear piezoelectricity is unconditionally stable, in which case Eqns (26) and (29) reduce to

$$\boldsymbol{a}_{n+1}^T \boldsymbol{M}\boldsymbol{a}_{n+1} + \boldsymbol{v}_{n+1}^T \boldsymbol{K}\boldsymbol{v}_{n+1} = \boldsymbol{a}_n^T \boldsymbol{B}\boldsymbol{a}_n + \boldsymbol{v}_n^T \boldsymbol{K}\boldsymbol{v}_n \tag{30}$$

$$\boldsymbol{a}_n^T \boldsymbol{M}\boldsymbol{a}_n + \boldsymbol{v}_n^T \boldsymbol{K}\boldsymbol{v}_n = \boldsymbol{a}_0^T \boldsymbol{M}\boldsymbol{a}_0 + \boldsymbol{v}_0^T \boldsymbol{K}\boldsymbol{v}_0, \qquad n = 1, 2, 3, \ldots \tag{31}$$

4.0 Partitioned Schemes

Applying the trapezoidal rule to the monolithic equation (22) yields the implicit unconditionally stable integration scheme, as described in the previous section:

$$\hat{\boldsymbol{K}}\boldsymbol{d}_{n+1} = \hat{\boldsymbol{F}}_{n+1}, \qquad \boldsymbol{v}_{n+1} = \frac{2}{\Delta t}(\boldsymbol{d}_{n+1} - \boldsymbol{d}_n) - \boldsymbol{v}_n \tag{32}$$

where

$$\hat{\boldsymbol{K}} = \boldsymbol{K} + \frac{4}{\Delta t^2}\boldsymbol{M}, \qquad \hat{\boldsymbol{F}}_{n+1} = \left(\frac{4}{\Delta t^2}\boldsymbol{M} - \boldsymbol{K}\right)\boldsymbol{d}_n + \frac{4}{\Delta t}\boldsymbol{M}\boldsymbol{v}_n + \boldsymbol{F}_n + \boldsymbol{F}_{n+1} \tag{33}$$

are the effective stiffness matrix and load vectors, respectively. First, we consider implicit partitioned schemes directly constructed from the above monolithic scheme and show that the resulting partitioned scheme is not unconditionally stable. Unconditionally stable

implicit partitioned scheme is then obtained via augmentation. An explicit partitioned scheme is also constructed from the explicit integration of mechanical equation.

4.1 Partitioning directly from the monolithic scheme

Partitioned schemes can be constructed directly from the monolithic scheme by splitting the effective stiffness matrix. The first equation of the monolithic scheme (32) can be written as

$$\begin{bmatrix} \hat{\boldsymbol{K}}_{\boldsymbol{uu}} & \boldsymbol{K}_{\boldsymbol{u}\phi} \\ \boldsymbol{K}_{\boldsymbol{u}\phi}^{\boldsymbol{T}} & -\boldsymbol{K}_{\phi\phi} \end{bmatrix} \begin{bmatrix} \boldsymbol{U}_{n+1} \\ \Phi_{n+1} \end{bmatrix} = \begin{bmatrix} \hat{\boldsymbol{F}}_{n+1}^{u} \\ \bar{\boldsymbol{Q}}_{n+1} \end{bmatrix} \tag{34}$$

where

$$\hat{\boldsymbol{K}}_{\boldsymbol{uu}} = \boldsymbol{K}_{\boldsymbol{uu}} + \frac{4}{\Delta t^2}\boldsymbol{M}_{\boldsymbol{uu}}, \qquad \hat{\boldsymbol{F}}_{n+1}^{u} = \boldsymbol{M}_{\boldsymbol{uu}}\left(\frac{4}{\Delta t^2}\boldsymbol{U}_n + \frac{4}{\Delta t}\dot{\boldsymbol{U}}_n + \ddot{\boldsymbol{U}}_n\right) + \bar{\boldsymbol{F}}_{n+1} \tag{35}$$

We start by considering a partitioned scheme where the electric field is predicted first. Splitting the coefficient matrix of (34) based on the block Gauss-Seidel method yields

$$\begin{bmatrix} \hat{\boldsymbol{K}}_{\boldsymbol{uu}} & \boldsymbol{0} \\ \boldsymbol{K}_{\boldsymbol{u}\phi}^{\boldsymbol{T}} & -\boldsymbol{K}_{\phi\phi} \end{bmatrix} \begin{bmatrix} \boldsymbol{U}_{n+1} \\ \Phi_{n+1} \end{bmatrix} = -\begin{bmatrix} \boldsymbol{0} & \boldsymbol{K}_{\boldsymbol{u}\phi} \\ \boldsymbol{0} & \boldsymbol{0} \end{bmatrix} \begin{bmatrix} \boldsymbol{U}_{n+1} \\ \Phi_{n+1} \end{bmatrix} + \begin{bmatrix} \hat{\boldsymbol{F}}_{n+1}^{u} \\ \bar{\boldsymbol{Q}}_{n+1} \end{bmatrix} \tag{36}$$

Utilizing the last-step-value predictor on the right hand side of (36), we have

$$\begin{bmatrix} \hat{\boldsymbol{K}}_{\boldsymbol{uu}} & \boldsymbol{0} \\ \boldsymbol{K}_{\boldsymbol{u}\phi}^{\boldsymbol{T}} & -\boldsymbol{K}_{\phi\phi} \end{bmatrix} \begin{bmatrix} \boldsymbol{U}_{n+1} \\ \Phi_{n+1} \end{bmatrix} = -\begin{bmatrix} \boldsymbol{0} & \boldsymbol{K}_{\boldsymbol{u}\phi} \\ \boldsymbol{0} & \boldsymbol{0} \end{bmatrix} \begin{bmatrix} \boldsymbol{U}_{n} \\ \Phi_{n} \end{bmatrix} + \begin{bmatrix} \hat{\boldsymbol{F}}_{n+1}^{u} \\ \bar{\boldsymbol{Q}}_{n+1} \end{bmatrix} \tag{37}$$

Expanding the above equation yields the electric field predicted partitioned scheme:

$$\hat{\boldsymbol{K}}_{\boldsymbol{uu}}\boldsymbol{U}_{n+1} = \hat{\boldsymbol{F}}_{n+1}^{u} - \boldsymbol{K}_{\boldsymbol{u}\phi}\Phi_n, \qquad \boldsymbol{K}_{\phi\phi}\Phi_{n+1} = -\bar{\boldsymbol{Q}}_{n+1} + \boldsymbol{K}_{\boldsymbol{u}\phi}^{\boldsymbol{T}}\boldsymbol{U}_{n+1} \tag{38}$$

Alternatively, we can predict the mechanical field. The monolithic equation (34) can be written as

$$\begin{bmatrix} -\boldsymbol{K}_{\phi\phi} & \boldsymbol{K}_{\boldsymbol{u}\phi}^{\boldsymbol{T}} \\ \boldsymbol{K}_{\boldsymbol{u}\phi} & \hat{\boldsymbol{K}}_{\boldsymbol{uu}} \end{bmatrix} \begin{bmatrix} \Phi_{n+1} \\ \boldsymbol{U}_{n+1} \end{bmatrix} = \begin{bmatrix} \bar{\boldsymbol{Q}}_{n+1} \\ \hat{\boldsymbol{F}}_{n+1}^{u} \end{bmatrix} \tag{39}$$

Splitting the coefficient matrix of the above equation based on the block Gauss-Seidel method yields

$$\begin{bmatrix} -\boldsymbol{K}_{\phi\phi} & \boldsymbol{0} \\ \boldsymbol{K}_{\boldsymbol{u}\phi} & \hat{\boldsymbol{K}}_{\boldsymbol{uu}} \end{bmatrix} \begin{bmatrix} \Phi_{n+1} \\ \boldsymbol{U}_{n+1} \end{bmatrix} = - \begin{bmatrix} \boldsymbol{0} & \boldsymbol{K}_{\boldsymbol{u}\phi}^{T} \\ \boldsymbol{0} & \boldsymbol{0} \end{bmatrix} \begin{bmatrix} \Phi_{n+1} \\ \boldsymbol{U}_{n+1} \end{bmatrix} + \begin{bmatrix} \overline{\boldsymbol{Q}}_{n+1} \\ \hat{\boldsymbol{F}}_{n+1}^{u} \end{bmatrix} \tag{40}$$

Utilizing the last-step-value predictor and expanding the resulting equation lead to the mechanical field predicted partitioned scheme

$$\boldsymbol{K}_{\phi\phi}\Phi_{n+1} = -\overline{\boldsymbol{Q}}_{n+1} + \boldsymbol{K}_{\boldsymbol{u}\phi}^{T}\boldsymbol{U}_{n}, \qquad \hat{\boldsymbol{K}}_{\boldsymbol{uu}}\boldsymbol{U}_{n+1} = \hat{\boldsymbol{F}}_{n+1}^{u} - \boldsymbol{K}_{\boldsymbol{u}\phi}\Phi_{n+1} \tag{41}$$

Both partitioned schemes solve the two field equations independently at each time step.

4.1.1 Stability analysis of the implicit partitioned schemes

Consider the partitioned procedures (38) and (41), which predict the electric field and mechanical field, respectively. Both partitioned procedures compute the velocity and acceleration fields based on the following equations:

$$\dot{\boldsymbol{U}}_{n+1} = \dot{\boldsymbol{U}}_{n} + \frac{\Delta t}{2}[\ddot{\boldsymbol{U}}_{n} + \boldsymbol{M}_{\boldsymbol{uu}}^{-1}(\overline{\boldsymbol{F}}_{n+1} - \boldsymbol{K}_{\boldsymbol{uu}}\boldsymbol{U}_{n+1} - \boldsymbol{K}_{\boldsymbol{u}\phi}\Phi_{n+1})] \tag{42}$$

$$\ddot{\boldsymbol{U}}_{n+1} = \boldsymbol{M}_{\boldsymbol{uu}}^{-1}(\overline{\boldsymbol{F}}_{n+1} - \boldsymbol{K}_{\boldsymbol{uu}}\boldsymbol{U}_{n+1} - \boldsymbol{K}_{\boldsymbol{u}\phi}\Phi_{n+1}) \tag{43}$$

For the purpose of stability analysis, it suffices to consider the force-free case, i.e., $\overline{\boldsymbol{F}}_{n+1} = \overline{\boldsymbol{Q}}_{n+1} = \boldsymbol{0}$. Stability analysis is carried using standard procedures[15][16]. Nontrivial solutions of the partitioned procedures are sought in the form

$$\boldsymbol{U}_{n+1} = \lambda\boldsymbol{U}_{n}, \quad \dot{\boldsymbol{U}}_{n+1} = \lambda\dot{\boldsymbol{U}}_{n}, \quad \ddot{\boldsymbol{U}}_{n+1} = \lambda\ddot{\boldsymbol{U}}_{n}, \quad \Phi_{n+1} = \lambda\Phi_{n} \tag{44}$$

Stability requires $|\lambda| \le 1$. When the modulus is unity, the root must be a simple one [17]. Replacing λ by $(1+z)/(1-z)$, stability condition reduces to

$$Re(z) \le 0 \tag{45}$$

First, we consider the mechanical field predicted partitioned procedure. Substituting Eqn (44) into (41)-(43) yields

$$\begin{bmatrix} -\dfrac{1+z}{1-z}\boldsymbol{K}_{\phi\phi} & \boldsymbol{K}_{\boldsymbol{u}\phi}^{T} \\ \boldsymbol{K}_{\boldsymbol{u}\phi} & \boldsymbol{K}_{\boldsymbol{uu}} + \dfrac{4z^{2}}{\Delta t^{2}}\boldsymbol{M}_{\boldsymbol{uu}} \end{bmatrix} \begin{bmatrix} \Phi_{n} \\ \boldsymbol{U}_{n} \end{bmatrix} = \boldsymbol{0} \tag{46}$$

The characteristic polynomial associated with (46) is

$$\left| z^3 \frac{4}{\Delta t^2} \boldsymbol{M}_{\boldsymbol{uu}} + z^2 \frac{4}{\Delta t^2} \boldsymbol{M}_{\boldsymbol{uu}} + z(\boldsymbol{K}_{\boldsymbol{uu}} - \boldsymbol{K}_{\boldsymbol{u}\phi} \boldsymbol{K}_{\phi\phi}^{-1} \boldsymbol{K}_{\boldsymbol{u}\phi}^T) + \boldsymbol{K}_{\boldsymbol{uu}} + \boldsymbol{K}_{\boldsymbol{u}\phi} \boldsymbol{K}_{\phi\phi}^{-1} \boldsymbol{K}_{\boldsymbol{u}\phi}^T \right| = 0 \tag{47}$$

where $|\ |$ denotes the matrix determinant. The necessary condition for stability is that all coefficient matrices of the polynomial in z should be positive definite (the first part of Routh-Hurwitz conditions [17][18]). Since $\boldsymbol{M}_{\boldsymbol{uu}}$ and $\boldsymbol{K}_{\boldsymbol{uu}} + \boldsymbol{K}_{\boldsymbol{u}\phi} \boldsymbol{K}_{\phi\phi}^{-1} \boldsymbol{K}_{\boldsymbol{u}\phi}^T$ are positive definite, but $\boldsymbol{K}_{\boldsymbol{uu}} - \boldsymbol{K}_{\boldsymbol{u}\phi} \boldsymbol{K}_{\phi\phi}^{-1} \boldsymbol{K}_{\boldsymbol{u}\phi}^T$ is indefinite, the necessary condition for stability cannot be satisfied.

Next, we investigate the electric field predicted partitioned scheme. Substituting Eqn (44) into (38), (42) and (43) yields

$$\begin{bmatrix} \boldsymbol{K}_{\phi\phi} & -\boldsymbol{K}_{\boldsymbol{u}\phi}^T \\ (1-z^2)\boldsymbol{K}_{\boldsymbol{u}\phi} & \boldsymbol{K}_{\boldsymbol{uu}} + \dfrac{4z^2}{\Delta t^2} \boldsymbol{M}_{\boldsymbol{uu}} \end{bmatrix} \begin{bmatrix} \Phi_n \\ \boldsymbol{U}_n \end{bmatrix} = \boldsymbol{0} \tag{48}$$

The characteristic polynomial of (48) is

$$\left| \left(\boldsymbol{M}_{\boldsymbol{uu}} - \frac{\Delta t^2}{4} \boldsymbol{K}_{\boldsymbol{u}\phi} \boldsymbol{K}_{\phi\phi}^{-1} \boldsymbol{K}_{\boldsymbol{u}\phi}^T \right) z^2 + \frac{\Delta t^2}{4} (\boldsymbol{K}_{\boldsymbol{uu}} + \boldsymbol{K}_{\boldsymbol{u}\phi} \boldsymbol{K}_{\phi\phi}^{-1} \boldsymbol{K}_{\boldsymbol{u}\phi}^T) \right| = 0 \tag{49}$$

To investigate the stability properties of the above equation it is convenient to utilize the theorem of Bellman [18], which states: If $\boldsymbol{A}$, $\boldsymbol{B}$ and $\boldsymbol{C}$ are non-negative definite, and either $\boldsymbol{A}$ or $\boldsymbol{C}$ positive definite, then

$$\left| z^2 \boldsymbol{A} + 2z\boldsymbol{B} + \boldsymbol{C} \right| = 0 \tag{50}$$

has no roots with positive real parts. The proof is given in [18].

In view of the above theorem, it is obvious that the necessary and sufficient condition for stability of the electric field predicted partitioned scheme is that the matrix $\boldsymbol{M}_{\boldsymbol{uu}} - \dfrac{\Delta t^2}{4} \boldsymbol{K}_{\boldsymbol{u}\phi} \boldsymbol{K}_{\phi\phi}^{-1} \boldsymbol{K}_{\boldsymbol{u}\phi}^T$ is non-negative definite, which can be achieved with sufficiently small Δt. Therefore, the scheme is conditionally stable.

We proceed to investigate the critical time step of the above scheme. Consider the eigenvalue problem

$$\left(\boldsymbol{M}_{\boldsymbol{uu}} - \frac{\Delta t^2}{4} \boldsymbol{K}_{\boldsymbol{u}\phi} \boldsymbol{K}_{\phi\phi}^{-1} \boldsymbol{K}_{\boldsymbol{u}\phi}^T \right) \boldsymbol{x} = \gamma \boldsymbol{x} \tag{51}$$

The necessary and sufficient condition for stability becomes

$$\gamma \geq 0 \tag{52}$$

From the generalized eigenvalue problem

$$[\boldsymbol{K}_{u\phi}\boldsymbol{K}_{\phi\phi}^{-1}\boldsymbol{K}_{u\phi}^{T} - (\omega^{im})^{2}\boldsymbol{M}_{uu}]\boldsymbol{x} = \boldsymbol{0} \tag{53}$$

we have

$$\boldsymbol{M}_{uu}^{-1}\boldsymbol{K}_{u\phi}\boldsymbol{K}_{\phi\phi}^{-1}\boldsymbol{K}_{u\phi}^{T}\boldsymbol{x} = (\omega^{im})^{2}\boldsymbol{x} \tag{54}$$

Premultiplying (51) by $\boldsymbol{M}_{uu}^{-1}$ yields

$$\boldsymbol{x} - \frac{\Delta t^{2}}{4}\boldsymbol{M}_{uu}^{-1}\boldsymbol{K}_{u\phi}\boldsymbol{K}_{\phi\phi}^{-1}\boldsymbol{K}_{u\phi}^{T}\boldsymbol{x} = \gamma\boldsymbol{M}_{uu}^{-1}\boldsymbol{x} \tag{55}$$

Substituting (54) into the above equation yields

$$\gamma\boldsymbol{M}_{uu}^{-1}\boldsymbol{x} = [1 - (\omega^{im}\Delta t)^{2}/4]\boldsymbol{x} \tag{56}$$

If $\gamma = 0$, we have from the above equation

$$\Delta t = 2/\omega^{im} \tag{57}$$

If $\gamma \neq 0$, we have from (56)

$$\boldsymbol{M}_{uu}^{-1}\boldsymbol{x} = \frac{[1 - (\omega^{im}\Delta t)^{2}/4]}{\gamma}\boldsymbol{x} \tag{58}$$

The positive definiteness of $\boldsymbol{M}_{uu}^{-1}$ and Eqn (52) lead to

$$1 - (\omega^{im}\Delta t)^{2}/4 > 0 \tag{59}$$

From Eqns (57) and (59), it follows that

$$\Delta t \leq 2/\omega^{im} \tag{60}$$

The above stability condition must be satisfied for each system mode. Consequently, the highest frequency ω_{n}^{im} is critical and must satisfy (60). Therefore, the stability condition becomes

$$\Delta t \leq \Delta t_{cr}^{im} = 2/\omega_{n}^{im} \tag{61}$$

4.1.2 Consistency and accuracy of the electric field predicted implicit scheme

By employing the equilibrium equation at t_n to eliminate $\ddot{\boldsymbol{U}}_n$, we can express the electric field predicted partitioned scheme (38), (42) and (43) in the following form

$$\delta_{n+1} = \boldsymbol{B}\delta_n + \boldsymbol{P}_n \tag{62}$$

where $\boldsymbol{B} = \boldsymbol{B}_1^{-1}\boldsymbol{B}_2$

$$\boldsymbol{B}_1 = \begin{bmatrix} \hat{\boldsymbol{K}}_{\boldsymbol{uu}} & \boldsymbol{0} & \boldsymbol{0} \\ \boldsymbol{K}_{\boldsymbol{u}\phi}^{\boldsymbol{T}} & \boldsymbol{0} & -\boldsymbol{K}_{\phi\phi} \\ \frac{\Delta t}{2}\boldsymbol{M}_{\boldsymbol{uu}}^{-1}\boldsymbol{K}_{\boldsymbol{uu}} & \boldsymbol{I} & \frac{\Delta t}{2}\boldsymbol{M}_{\boldsymbol{uu}}^{-1}\boldsymbol{K}_{\boldsymbol{u}\phi} \end{bmatrix}, \quad \boldsymbol{B}_2 = \begin{bmatrix} \frac{4}{\Delta t^2}\boldsymbol{M}_{\boldsymbol{uu}} - \boldsymbol{K}_{\boldsymbol{uu}} & \frac{4}{\Delta t}\boldsymbol{M}_{\boldsymbol{uu}} & -2\boldsymbol{K}_{\boldsymbol{u}\phi} \\ \boldsymbol{0} & \boldsymbol{0} & \boldsymbol{0} \\ -\frac{\Delta t}{2}\boldsymbol{M}_{\boldsymbol{uu}}^{-1}\boldsymbol{K}_{\boldsymbol{uu}} & \boldsymbol{I} & -\frac{\Delta t}{2}\boldsymbol{M}_{\boldsymbol{uu}}^{-1}\boldsymbol{K}_{\boldsymbol{u}\phi} \end{bmatrix}$$

$$\delta_n = \begin{bmatrix} \boldsymbol{U}_n \\ \dot{\boldsymbol{U}}_n \\ \Phi_n \end{bmatrix}, \qquad \boldsymbol{P}_n = \boldsymbol{B}_1^{-1}\begin{bmatrix} \overline{\boldsymbol{F}}_n + \overline{\boldsymbol{F}}_{n+1} \\ \overline{\boldsymbol{Q}}_{n+1} \\ \frac{\Delta t}{2}\boldsymbol{M}_{\boldsymbol{uu}}^{-1}(\overline{\boldsymbol{F}}_n + \overline{\boldsymbol{F}}_{n+1}) \end{bmatrix} \tag{63}$$

Inserting the exact solution $\delta(t_n)$ into (62), we have

$$\delta(t_{n+1}) = \boldsymbol{B}\delta(t_n) + \boldsymbol{P}_n + \Re(t_n) \tag{64}$$

where $\Re(t_n) = \left[\Re_u^T(t_n) \;\; \dot{\Re}_u^T(t_n) \;\; \Re_\phi^T(t_n)\right]^T$ is the local truncation error. Inserting the following Taylor expansions

$$\delta(t_{n+1}) = \delta(t_n) + \Delta t\dot{\delta}(t_n) + \frac{\Delta t^2}{2}\ddot{\delta}(t_n) + \frac{\Delta t^3}{6}\dddot{\delta}(t_n) + O(\Delta t^4) \tag{65}$$

$$\overline{\boldsymbol{F}}_{n+1} = \overline{\boldsymbol{F}}_n + \Delta t\dot{\overline{\boldsymbol{F}}}_n + \frac{\Delta t^2}{2}\ddot{\overline{\boldsymbol{F}}}_n + \frac{\Delta t^3}{6}\dddot{\overline{\boldsymbol{F}}}_n + O(\Delta t^4) \tag{66}$$

$$\overline{\boldsymbol{Q}}_{n+1} = \overline{\boldsymbol{Q}}_n + \Delta t\dot{\overline{\boldsymbol{Q}}}_n + \frac{\Delta t^2}{2}\ddot{\overline{\boldsymbol{Q}}}_n + \frac{\Delta t^3}{6}\dddot{\overline{\boldsymbol{Q}}}_n + O(\Delta t^4) \tag{67}$$

into Eqn (64) and expanding the resulting equation, it can be shown that

$$\Re(t_n) \sim O(\Delta t^3) \text{ and } \Re(t_n) \to 0 \text{ as } \Delta t \to 0 \tag{68}$$

Therefore, the electric field predicted partitioned scheme is consistent and second-order accurate.

4.2 Unconditionally stable implicit partitioned scheme

4.2.1 Stabilization by semi-algebraic augmentation

The stabilization is carried out by a semi-algebraic augmentation technique proposed by Farhat, Park and Pelerin[15] for thermoelastic problems.

First, the structural equation in (18) is integrated using the trapezoidal rule:

$$\dot{\boldsymbol{U}}_{n+1} = \dot{\boldsymbol{U}}_n + \frac{\Delta t}{2}(\ddot{\boldsymbol{U}}_n + \ddot{\boldsymbol{U}}_{n+1})$$

$$= \dot{\boldsymbol{U}}_n + \frac{\Delta t}{2}[\ddot{\boldsymbol{U}}_n + \boldsymbol{M}_{\boldsymbol{uu}}^{-1}(\overline{\boldsymbol{F}}_{n+1} - \boldsymbol{K}_{\boldsymbol{uu}}\boldsymbol{U}_{n+1} - \boldsymbol{K}_{\boldsymbol{u}\phi}\Phi_{n+1})] \tag{69}$$

$$\boldsymbol{U}_{n+1} = \boldsymbol{U}_n + \Delta t\dot{\boldsymbol{U}}_n + \frac{\Delta t^2}{4}(\ddot{\boldsymbol{U}}_n + \ddot{\boldsymbol{U}}_{n+1})$$

$$= \boldsymbol{U}_n + \Delta t\dot{\boldsymbol{U}}_n + \frac{\Delta t^2}{4}[\ddot{\boldsymbol{U}}_n + \boldsymbol{M}_{\boldsymbol{uu}}^{-1}(\overline{\boldsymbol{F}}_{n+1} - \boldsymbol{K}_{\boldsymbol{uu}}\boldsymbol{U}_{n+1} - \boldsymbol{K}_{\boldsymbol{u}\phi}\Phi_{n+1})] \tag{70}$$

Consider the electric equation

$$\boldsymbol{K}_{\boldsymbol{u}\phi}^T\boldsymbol{U}_{n+1} - \boldsymbol{K}_{\phi\phi}\Phi_{n+1} = \overline{\boldsymbol{Q}}_{n+1} \tag{71}$$

Substituting Eqn (70) into the above equation yields

$$\hat{\boldsymbol{K}}_{\phi\boldsymbol{u}}\boldsymbol{U}_{n+1} + \hat{\boldsymbol{K}}_{\phi\phi}\Phi_{n+1} = \hat{\boldsymbol{F}}_{n+1}^{\phi} \tag{72}$$

where

$$\hat{\boldsymbol{K}}_{\phi\boldsymbol{u}} = \frac{\Delta t^2}{4}\boldsymbol{K}_{\boldsymbol{u}\phi}^T\boldsymbol{M}_{\boldsymbol{uu}}^{-1}\boldsymbol{K}_{\boldsymbol{uu}}, \qquad \hat{\boldsymbol{K}}_{\phi\phi} = \boldsymbol{K}_{\phi\phi} + \frac{\Delta t^2}{4}\boldsymbol{K}_{\boldsymbol{u}\phi}^T\boldsymbol{M}_{\boldsymbol{uu}}^{-1}\boldsymbol{K}_{\boldsymbol{u}\phi}$$

$$\hat{\boldsymbol{F}}_{n+1}^{\phi} = \frac{\Delta t^2}{4}\boldsymbol{K}_{\boldsymbol{u}\phi}^T\boldsymbol{M}_{\boldsymbol{uu}}^{-1}\overline{\boldsymbol{F}}_{n+1} + \boldsymbol{K}_{\boldsymbol{u}\phi}^T\left(\boldsymbol{U}_n + \Delta t\dot{\boldsymbol{U}}_n + \frac{\Delta t^2}{4}\ddot{\boldsymbol{U}}_n\right) - \overline{\boldsymbol{Q}}_{n+1} \tag{73}$$

Rearranging (70) yields

$$\hat{\boldsymbol{K}}_{\boldsymbol{uu}}\boldsymbol{U}_{n+1} + \boldsymbol{K}_{\boldsymbol{u}\phi}\Phi_{n+1} = \hat{\boldsymbol{F}}_{n+1}^{u} \tag{74}$$

where $\hat{\boldsymbol{K}}_{\boldsymbol{uu}}$ and $\hat{\boldsymbol{F}}_{n+1}^{u}$ are given in (35). Equations (72) and (74) can be written as

$$\begin{bmatrix} \hat{\boldsymbol{K}}_{\phi\phi} & \hat{\boldsymbol{K}}_{\phi \boldsymbol{u}} \\ \boldsymbol{K}_{\boldsymbol{u}\phi} & \hat{\boldsymbol{K}}_{\boldsymbol{uu}} \end{bmatrix} \begin{bmatrix} \Phi_{n+1} \\ \boldsymbol{U}_{n+1} \end{bmatrix} = \begin{bmatrix} \hat{\boldsymbol{F}}^{\phi}_{n+1} \\ \hat{\boldsymbol{F}}^{u}_{n+1} \end{bmatrix} \tag{75}$$

Splitting the coefficient matrix in (75) using the block Gauss-Seidel method and last-step-value predictor, we have

$$\begin{bmatrix} \hat{\boldsymbol{K}}_{\phi\phi} & \boldsymbol{0} \\ \boldsymbol{K}_{\boldsymbol{u}\phi} & \hat{\boldsymbol{K}}_{\boldsymbol{uu}} \end{bmatrix} \begin{bmatrix} \Phi_{n+1} \\ \boldsymbol{U}_{n+1} \end{bmatrix} = -\begin{bmatrix} \boldsymbol{0} & \hat{\boldsymbol{K}}_{\phi \boldsymbol{u}} \\ \boldsymbol{0} & \boldsymbol{0} \end{bmatrix} \begin{bmatrix} \Phi_{n} \\ \boldsymbol{U}_{n} \end{bmatrix} + \begin{bmatrix} \hat{\boldsymbol{F}}^{\phi}_{n+1} \\ \hat{\boldsymbol{F}}^{u}_{n+1} \end{bmatrix} \tag{76}$$

Expanding the above equation and using (69) yield the following partitioned algorithm:

1. Predict the mechanical filed

$$\boldsymbol{U}^{p}_{n+1} = \boldsymbol{U}_{n} \tag{77}$$

2. Solve for the electric field

$$\hat{\boldsymbol{K}}_{\phi\phi} \Phi_{n+1} = \hat{\boldsymbol{F}}^{\phi}_{n+1} - \hat{\boldsymbol{K}}_{\phi \boldsymbol{u}} \boldsymbol{U}^{p}_{n+1} \tag{78}$$

3. Correct the mechanical field

$$\hat{\boldsymbol{K}}_{\boldsymbol{uu}} \boldsymbol{U}_{n+1} = \hat{\boldsymbol{F}}^{u}_{n+1} - \boldsymbol{K}_{\boldsymbol{u}\phi} \Phi_{n+1} \tag{79}$$

4. Compute velocity and acceleration fields

$$\dot{\boldsymbol{U}}_{n+1} = \dot{\boldsymbol{U}}_{n} + \frac{\Delta t}{2}[\ddot{\boldsymbol{U}}_{n} + \boldsymbol{M}^{-1}_{\boldsymbol{uu}}(\overline{\boldsymbol{F}}_{n+1} - \boldsymbol{K}_{\boldsymbol{uu}} \boldsymbol{U}_{n+1} - \boldsymbol{K}_{\boldsymbol{u}\phi} \Phi_{n+1})] \tag{80}$$

$$\ddot{\boldsymbol{U}}_{n+1} = \boldsymbol{M}^{-1}_{\boldsymbol{uu}}(\overline{\boldsymbol{F}}_{n+1} - \boldsymbol{K}_{\boldsymbol{uu}} \boldsymbol{U}_{n+1} - \boldsymbol{K}_{\boldsymbol{u}\phi} \Phi_{n+1}) \tag{81}$$

4.2.2 Stability and accuracy of the stabilized implicit scheme

Stability. We consider the force-free case, i.e. $\overline{\boldsymbol{F}}_{n+1} = \overline{\boldsymbol{Q}}_{n+1} = \boldsymbol{0}$. The stability of the proposed partitioned scheme can be examined by seeking a non-trivial solution in the form of (44). Substituting (77) into (78), and (44) into (78)-(81), we have after some algebraic manipulations

$$\begin{bmatrix} \boldsymbol{K}_{uu} + \dfrac{4z^2}{\Delta t^2}\boldsymbol{M}_{uu} & \boldsymbol{K}_{u\phi} \\ \dfrac{\Delta t^2}{2}(1-z^2)\boldsymbol{V}\boldsymbol{K}_{uu} - z(1-z)\boldsymbol{K}_{\phi\phi}^{-1}\boldsymbol{K}_{u\phi}^T & z(z+1)\boldsymbol{I} + \dfrac{\Delta t^2}{2}\boldsymbol{V}\boldsymbol{K}_{u\phi} \end{bmatrix} \begin{bmatrix} \boldsymbol{U}_n \\ \Phi_n \end{bmatrix} = \boldsymbol{0} \tag{82}$$

where

$$\boldsymbol{V} = \boldsymbol{K}_{\phi\phi}^{-1}\boldsymbol{K}_{u\phi}^T\boldsymbol{M}_{uu}^{-1} \tag{83}$$

The characteristic polynomial associated with (82) is

$$\det\left\{ \boldsymbol{M}_{uu}z^3 + \boldsymbol{M}_{uu}z^2 + \frac{\Delta t^2 z}{4}\left[\boldsymbol{K}_{uu} + \boldsymbol{K}_{u\phi}\boldsymbol{K}_{\phi\phi}^{-1}\boldsymbol{K}_{u\phi}^T\left(\boldsymbol{I} + \frac{\Delta t^2}{2}\boldsymbol{M}_{uu}^{-1}\boldsymbol{K}_{uu} \right) \right] + \right.$$

$$\left. \frac{\Delta t^2}{4}(\boldsymbol{K}_{uu} + \boldsymbol{K}_{u\phi}\boldsymbol{K}_{\phi\phi}^{-1}\boldsymbol{K}_{u\phi}^T) \right\} = 0 \tag{84}$$

Recall that $\boldsymbol{M}_{uu}$, $\boldsymbol{K}_{uu}$ and $\boldsymbol{K}_{\phi\phi}$ are positive definite; $\boldsymbol{K}_{u\phi}\boldsymbol{K}_{\phi\phi}^{-1}\boldsymbol{K}_{u\phi}^T$ is positive definite provided that $\boldsymbol{K}_{u\phi}$ has full column rank and positive semi-definite if $\boldsymbol{K}_{u\phi}$ is column rank deficient. In any case, all coefficient matrices of the characteristic polynomial (84) are positive definite. Therefore, the first part of the Routh-Hurwitz criterion for unconditional stability is satisfied. In order to check the second part of this criterion, we consider a 2-dof model problem. The corresponding scalar form of (84) is

$$a_3z^3 + a_2z^2 + a_1z + a_0 = 0 \tag{85}$$

where

$$a_3 = a_2 = 1, \quad a_1 = \frac{\Delta t^2}{4}\left[\omega^2 + \frac{e^2}{m\varphi}\left(1 + \frac{\Delta t^2}{2}\omega^2 \right) \right], \quad a_0 = \frac{\Delta t^2}{4}\left(\omega^2 + \frac{e^2}{m\varphi} \right) \tag{86}$$

Since Δt, φ, ω^2, e^2 and $m > 0$, all coefficients of the polynomial (85) are positive. Moreover

$$a_1a_2 - a_0a_3 = \frac{\Delta t^4}{8}\frac{e^2\omega^2}{m\varphi} > 0 \tag{87}$$

which verifies that the second part of the Routh-Hurwitz criterion is satisfied and therefore the partitioned procedure is unconditionally stable.

Consistency and Accuracy. Using the equilibrium equation at t_n to eliminate $\ddot{\boldsymbol{U}}_n$ in expressions (35), (73) and (80) for $\hat{\boldsymbol{F}}^{u}_{n+1}$, $\hat{\boldsymbol{F}}^{\phi}_{n+1}$ and $\dot{\boldsymbol{U}}_{n+1}$, respectively, and substituting the resulting effective load vectors into (78) and (79), then writing the resulting equations in a matrix form yield

$$\delta_{n+1} = \boldsymbol{R}\delta_n + \bar{\boldsymbol{L}}_n \tag{88}$$

where δ_n is given in (63) and

$$\boldsymbol{R} = \boldsymbol{R}_1^{-1}\boldsymbol{R}_2, \qquad \bar{\boldsymbol{L}}_n = \boldsymbol{R}_1^{-1}\boldsymbol{L}' \tag{89}$$

$$\boldsymbol{R}_1 = \begin{bmatrix} \boldsymbol{I} + \Delta t^2 \boldsymbol{M}_{\boldsymbol{uu}}^{-1}\boldsymbol{K}_{\boldsymbol{uu}}/4 & \boldsymbol{0} & \Delta t^2 \boldsymbol{M}_{\boldsymbol{uu}}^{-1}\boldsymbol{K}_{\boldsymbol{u}\phi}/4 \\ \Delta t \boldsymbol{M}_{\boldsymbol{uu}}^{-1}\boldsymbol{K}_{\boldsymbol{uu}}/2 & \boldsymbol{I} & \Delta t \boldsymbol{M}_{\boldsymbol{uu}}^{-1}\boldsymbol{K}_{\boldsymbol{u}\phi}/2 \\ \boldsymbol{0} & \boldsymbol{0} & \boldsymbol{K}_{\phi\phi} + \Delta t^2 \boldsymbol{K}_{\boldsymbol{u}\phi}^{T}\boldsymbol{M}_{\boldsymbol{uu}}^{-1}\boldsymbol{K}_{\boldsymbol{u}\phi}/4 \end{bmatrix}$$

$$\boldsymbol{R}_2 = \begin{bmatrix} \boldsymbol{I} - \Delta t^2 \boldsymbol{M}_{\boldsymbol{uu}}^{-1}\boldsymbol{K}_{\boldsymbol{uu}}/4 & \Delta t \boldsymbol{I} & -\Delta t^2 \boldsymbol{M}_{\boldsymbol{uu}}^{-1}\boldsymbol{K}_{\boldsymbol{u}\phi}/4 \\ -\Delta t \boldsymbol{M}_{\boldsymbol{uu}}^{-1}\boldsymbol{K}_{\boldsymbol{uu}}/2 & \boldsymbol{I} & -\Delta t \boldsymbol{M}_{\boldsymbol{uu}}^{-1}\boldsymbol{K}_{\boldsymbol{u}\phi}/2 \\ \boldsymbol{K}_{\boldsymbol{u}\phi}^{T} - \Delta t^2 \boldsymbol{K}_{\boldsymbol{u}\phi}^{T}\boldsymbol{M}_{\boldsymbol{uu}}^{-1}\boldsymbol{K}_{\boldsymbol{uu}}/2 & \Delta t \boldsymbol{K}_{\boldsymbol{u}\phi}^{T} & -\Delta t^2 \boldsymbol{K}_{\boldsymbol{u}\phi}^{T}\boldsymbol{M}_{\boldsymbol{uu}}^{-1}\boldsymbol{K}_{\boldsymbol{u}\phi}/4 \end{bmatrix}$$

$$\boldsymbol{L}' = \begin{bmatrix} \Delta t^2 \boldsymbol{M}_{\boldsymbol{uu}}^{-1}(\bar{\boldsymbol{F}}_n + \bar{\boldsymbol{F}}_{n+1})/4 \\ \Delta t \boldsymbol{M}_{\boldsymbol{uu}}^{-1}(\bar{\boldsymbol{F}}_n + \bar{\boldsymbol{F}}_{n+1})/2 \\ \Delta t^2 \boldsymbol{K}_{\boldsymbol{u}\phi}^{T}\boldsymbol{M}_{\boldsymbol{uu}}^{-1}(\bar{\boldsymbol{F}}_n + \bar{\boldsymbol{F}}_{n+1})/4 - \bar{\boldsymbol{Q}}_{n+1} \end{bmatrix} \tag{90}$$

Inserting the solution $\delta(t_n)$ into (88), we have

$$\delta(t_{n+1}) = \boldsymbol{R}\delta(t_n) + \bar{\boldsymbol{L}}_n + \tau(t_n) \tag{91}$$

where $\tau(t_n) = \left[\tau_u^T(t_n)\ \dot{\tau}_u^T(t_n)\ \tau_\phi(t_n)\right]^T$ is the local truncation error. Inserting the Taylor expansions (65) - (67) into (91) and expanding the resulting equation yield

$$\tau_u(t_n) \sim O(\Delta t^3), \qquad \dot{\tau}_u(t_n) \sim O(\Delta t^3). \qquad \tau_\phi(t_n) \sim O(\Delta t^3) \tag{92}$$

$$\tau(t_n) \sim O(\Delta t^3) \text{ and } \tau(t_n) \to 0 \text{ as } \Delta t \to 0 \tag{93}$$

Therefore, the partitioned scheme is consistent and second-order accurate.

4.3 Explicit partitioned scheme

The explicit partitioned scheme can be also constructed by integrating the mechanical equation directly using an explicit integrator, e.g. the central difference scheme for the velocity and acceleration fields

$$\dot{\boldsymbol{U}}_n = \frac{1}{2\Delta t}(\boldsymbol{U}_{n+1} - \boldsymbol{U}_{n-1}), \qquad \ddot{\boldsymbol{U}}_n = \frac{1}{\Delta t^2}(\boldsymbol{U}_{n+1} - 2\boldsymbol{U}_n + \boldsymbol{U}_{n-1}) \tag{94}$$

The mechanical equation of motion at t_n is

$$\boldsymbol{M}_{\boldsymbol{uu}}\ddot{\boldsymbol{U}}_n + \boldsymbol{K}_{\boldsymbol{uu}}\boldsymbol{U}_n + \boldsymbol{K}_{\boldsymbol{u}\phi}\Phi_n = \bar{\boldsymbol{F}}_n \tag{95}$$

Substituting the second equation in (94) into (95) yields

$$\frac{1}{\Delta t^2}\boldsymbol{M}_{\boldsymbol{uu}}\boldsymbol{U}_{n+1} = \hat{\boldsymbol{P}}_n \tag{96}$$

where

$$\hat{\boldsymbol{P}}_n = \bar{\boldsymbol{F}}_n + \left(\frac{2}{\Delta t^2}\boldsymbol{M}_{\boldsymbol{uu}} - \boldsymbol{K}_{\boldsymbol{uu}}\right)\boldsymbol{U}_n - \frac{1}{\Delta t^2}\boldsymbol{M}_{\boldsymbol{uu}}\boldsymbol{U}_{n-1} - \boldsymbol{K}_{\boldsymbol{u}\phi}\Phi_n \tag{97}$$

The resulting algorithm for the explicit partitioned scheme is:

1. Evaluate the mechanical field by Eqn (96). Note that if lumped mass matrix is employed, there is no solution of equations for the mechanical field.

2. Evaluate the electric field by

$$\boldsymbol{K}_{\phi\phi}\Phi_{n+1} = \boldsymbol{K}_{\boldsymbol{u}\phi}^T\boldsymbol{U}_{n+1} - \bar{\boldsymbol{Q}}_{n+1} \tag{98}$$

3. If required, compute the velocity and acceleration fields at t_n using Eqn (94).

Based on Eqn (94), the starting value of displacements is taken as

$$\boldsymbol{U}_{-1} = \boldsymbol{U}_0 - \Delta t\dot{\boldsymbol{U}}_0 + \frac{\Delta t^2}{2}\ddot{\boldsymbol{U}}_0 \tag{99}$$

4.3.1 Stability of the explicit partitioned scheme

As before, we seek for a non-trivial solution in the form of (44). Substituting Eqn (97) into (96) and (44) into (96) and (98) yields

$$\begin{bmatrix} -\boldsymbol{K}_{\phi\phi} & \boldsymbol{K}_{\boldsymbol{u}\phi}^T \\ \boldsymbol{K}_{\boldsymbol{u}\phi} & \boldsymbol{K}_{\boldsymbol{uu}} + \dfrac{4z^2}{(1-z^2)\Delta t^2}\boldsymbol{M}_{\boldsymbol{uu}} \end{bmatrix} \begin{bmatrix} \Phi_n \\ \boldsymbol{U}_n \end{bmatrix} = \boldsymbol{0} \tag{100}$$

The characteristic polynomial of (100) is

$$\det\left\{ z^2\left[\boldsymbol{M}_{\boldsymbol{uu}} - \frac{\Delta t^2}{4}(\boldsymbol{K}_{\boldsymbol{uu}} + \boldsymbol{K}_{\boldsymbol{u}\phi}\boldsymbol{K}_{\phi\phi}^{-1}\boldsymbol{K}_{\boldsymbol{u}\phi}^T) \right] + \frac{\Delta t^2}{4}(\boldsymbol{K}_{\boldsymbol{uu}} + \boldsymbol{K}_{\boldsymbol{u}\phi}\boldsymbol{K}_{\phi\phi}^{-1}\boldsymbol{K}_{\boldsymbol{u}\phi}^T) \right\} = 0 \tag{101}$$

Since $\boldsymbol{K}_{\boldsymbol{uu}} + \boldsymbol{K}_{\boldsymbol{u}\phi}\boldsymbol{K}_{\phi\phi}^{-1}\boldsymbol{K}_{\boldsymbol{u}\phi}^T$ is positive definite, by the theorem of Bellman, the stability condition of the explicit partitioned scheme becomes

$$\boldsymbol{M}_{\boldsymbol{uu}} - \frac{\Delta t^2}{4}(\boldsymbol{K}_{\boldsymbol{uu}} + \boldsymbol{K}_{\boldsymbol{u}\phi}\boldsymbol{K}_{\phi\phi}^{-1}\boldsymbol{K}_{\boldsymbol{u}\phi}^T) \geq \boldsymbol{0} \tag{102}$$

By similar arguments described in Section ***4.1.1,*** it follows that the explicit partitioned scheme is conditionally stable and the condition for stability is governed by

$$\Delta t \leq \Delta t_{cr}^{ex} = 2/\omega_n^{ex} \tag{103}$$

where ω_n^{ex} is the largest value of the following generalized eigenvalue problem

$$[(\boldsymbol{K}_{\boldsymbol{uu}} + \boldsymbol{K}_{\boldsymbol{u}\phi}\boldsymbol{K}_{\phi\phi}^{-1}\boldsymbol{K}_{\boldsymbol{u}\phi}^T) - (\omega^{ex})^2\boldsymbol{M}_{\boldsymbol{uu}}]\boldsymbol{x} = \boldsymbol{0} \tag{104}$$

Since $\boldsymbol{K}_{\boldsymbol{uu}}$ is positive definite, by comparing Eqns (53) and (104), we have

$$\omega_n^{ex} > \omega_n^{im}, \text{ and thus } \Delta t_{cr}^{ex} < \Delta t_{cr}^{im} \tag{105}$$

4.3.2 Consistency and accuracy

Substituting Eqn (97) into (96) and (98), we have

$$\boldsymbol{y}_{n+1} = \boldsymbol{A}_1\boldsymbol{y}_n + \boldsymbol{A}_2\boldsymbol{y}_{n-1} + \boldsymbol{L}_n \tag{106}$$

where

$$\boldsymbol{y}_n = \begin{bmatrix} \boldsymbol{U}_n \\ \Phi_n \end{bmatrix}, \qquad \boldsymbol{A}_1 = \begin{bmatrix} 2\boldsymbol{I} - \Delta t^2\boldsymbol{M}_{\boldsymbol{uu}}^{-1}\boldsymbol{K}_{\boldsymbol{uu}} & -\Delta t^2\boldsymbol{M}_{\boldsymbol{uu}}^{-1}\boldsymbol{K}_{\boldsymbol{u}\phi} \\ \boldsymbol{K}_{\phi\phi}^{-1}\boldsymbol{K}_{\boldsymbol{u}\phi}^{\boldsymbol{T}}(2\boldsymbol{I} - \Delta t^2\boldsymbol{M}_{\boldsymbol{uu}}^{-1}\boldsymbol{K}_{\boldsymbol{uu}}) & -\Delta t^2\boldsymbol{K}_{\phi\phi}^{-1}\boldsymbol{K}_{\boldsymbol{u}\phi}^{\boldsymbol{T}}\boldsymbol{M}_{\boldsymbol{uu}}^{-1}\boldsymbol{K}_{\boldsymbol{u}\phi} \end{bmatrix} \tag{107}$$

$$\boldsymbol{A}_2 = \begin{bmatrix} -\boldsymbol{I} & \boldsymbol{0} \\ -\boldsymbol{K}_{\phi\phi}^{-1}\boldsymbol{K}_{\boldsymbol{u}\phi}^{\boldsymbol{T}} & \boldsymbol{0} \end{bmatrix}, \qquad \boldsymbol{L}_n = \begin{bmatrix} \Delta t^2 \boldsymbol{M}_{\boldsymbol{uu}}^{-1}\overline{\boldsymbol{F}}_n \\ \Delta t^2 \boldsymbol{K}_{\phi\phi}^{-1}\boldsymbol{K}_{\boldsymbol{u}\phi}^{\boldsymbol{T}}\boldsymbol{M}_{\boldsymbol{uu}}^{-1}\overline{\boldsymbol{F}}_n - \boldsymbol{K}_{\phi\phi}^{-1}\overline{\boldsymbol{Q}}_{n+1} \end{bmatrix} \tag{108}$$

Inserting the exact solution $\boldsymbol{y}(t_n)$ into (106) yields

$$\boldsymbol{y}(t_{n+1}) = \boldsymbol{A}_1\boldsymbol{y}(t_n) + \boldsymbol{A}_2\boldsymbol{y}(t_{n-1}) + \boldsymbol{L}_n + \boldsymbol{r}(t_n) \tag{109}$$

where $\boldsymbol{r}(t_n) = \left[\boldsymbol{r}_{\boldsymbol{u}}^T(t_n)\ \boldsymbol{r}_{\phi}^T(t_n)\right]^T$ is the local truncation error. Inserting the Taylor expansions

$$\boldsymbol{y}(t_{n+1}) = \boldsymbol{y}(t_n) + \Delta t\dot{\boldsymbol{y}}(t_n) + \frac{\Delta t^2}{2}\ddot{\boldsymbol{y}}(t_n) + \frac{\Delta t^3}{6}\dddot{\boldsymbol{y}}(t_n) + O(\Delta t^4) \tag{110}$$

$$\boldsymbol{y}(t_{n-1}) = \boldsymbol{y}(t_n) - \Delta t\dot{\boldsymbol{y}}(t_n) + \frac{\Delta t^2}{2}\ddot{\boldsymbol{y}}(t_n) - \frac{\Delta t^3}{6}\dddot{\boldsymbol{y}}(t_n) + O(\Delta t^4) \tag{111}$$

and (67) into (109), yield

$$\boldsymbol{r}_{\boldsymbol{u}}(t_n) \sim O(\Delta t^4), \qquad \boldsymbol{r}_{\phi}(t_n) \sim O(\Delta t^4) \tag{112}$$

Substituting the exact solutions into (94), we have

$$\dot{\boldsymbol{U}}(t_n) = \frac{1}{2\Delta t}[\boldsymbol{U}(t_{n+1}) - \boldsymbol{U}(t_{n-1})] + \dot{\boldsymbol{r}}_{\boldsymbol{u}}(t_n) \tag{113}$$

$$\ddot{\boldsymbol{U}}(t_n) = \frac{1}{\Delta t^2}[\boldsymbol{U}(t_{n+1}) - 2\boldsymbol{U}(t_n) + \boldsymbol{U}(t_{n-1})] + \ddot{\boldsymbol{r}}_{\boldsymbol{u}}(t_n) \tag{114}$$

where $\dot{\boldsymbol{r}}_{\boldsymbol{u}}(t_n)$ and $\ddot{\boldsymbol{r}}_{\boldsymbol{u}}(t_n)$ are local truncation errors in velocity and acceleration, respectively. Substituting the expansions (110) and (111) into (113) and (114), yield

$$\dot{\boldsymbol{r}}_{\boldsymbol{u}}(t_n) \sim O(\Delta t^2), \qquad \ddot{\boldsymbol{r}}_{\boldsymbol{u}}(t_n) \sim O(\Delta t^2) \tag{115}$$

The truncation errors vanish as $\Delta t \to 0$. Therefore, the explicit partitioned scheme is consistent.

5.0 The RVE-based Multilevel Method for Partitioned Scheme

The explicit and implicit conditionally stable as well as implicit unconditionally stable partitioned schemes proposed in the previous section entail solving linear systems of equations at each time station. Attention is restricted to piezocomposites where the size of the microstructure is comparable to that of the wavelength of a traveling signal necessitat-

ing discretization on the scale of heterogeneity. The classical multigrid approach with standard linear interpolation operators applied to the resulting discrete system has been show to exhibit poor rate of convergence, mainly because the lower frequency subspace is not geometrically smooth for problems in heterogeneous media [6].

We focus on the RVE-based multilevel method developed by the authors for structural dynamics problems [6], in which the special intergrid transfer operators are constructed from the solution of the Representative Volume Element (RVE). The so called RVE-based multilevel approach has been shown to possess an increasing rate of convergence with increase in mismatch of properties between microconstituents and decrease in time step size. In the case of homogeneous media and static analysis, the method has been shown to recover the rate of convergence of the classic multigrid method, i.e., $1/3$.

We note that in the mechanical field equations (38) and (79), the coefficient matrix is identical to that obtained from the conventional structural dynamics problems. Convergence characteristics of the RVE-based multilevel method for mechanical equations has been studied in [6]. In the remaining of this section attention is restricted on convergence studies of the RVE-based multilevel method applied to the electric field equations (38) or (98), and (78).

5.1 Two-level iteration matrices

We consider the two-level iteration process consisting of υ SSOR pre- and post-smoothing iterations. The coarse-model dielectric and effective dielectric stiffness matrices are obtained by restricting the corresponding source grid matrices:

$$\boldsymbol{K}_{0\phi\phi} = \boldsymbol{Q}^T \boldsymbol{K}_{\phi\phi} \boldsymbol{Q}, \qquad \hat{\boldsymbol{K}}_{0\phi\phi} = \tilde{\boldsymbol{Q}}^T \hat{\boldsymbol{K}}_{\phi\phi} \tilde{\boldsymbol{Q}} \tag{116}$$

where $\boldsymbol{Q}$ and $\tilde{\boldsymbol{Q}}$ are the prolongation operators for the corresponding electric equations. The resulting two-level iteration matrices are given by

$$\boldsymbol{L}_{\phi\phi} = \boldsymbol{S}_{\phi\phi}^{\upsilon} \boldsymbol{T}_{\phi\phi} \boldsymbol{S}_{\phi\phi}^{\upsilon}, \qquad \hat{\boldsymbol{L}}_{\phi\phi} = \hat{\boldsymbol{S}}_{\phi\phi}^{\upsilon} \hat{\boldsymbol{T}}_{\phi\phi} \hat{\boldsymbol{S}}_{\phi\phi}^{\upsilon} \tag{117}$$

where

$$\boldsymbol{S}_{\phi\phi} = \boldsymbol{I} - \boldsymbol{P}_{\phi\phi}^{-1} \boldsymbol{K}_{\phi\phi}, \qquad \hat{\boldsymbol{S}}_{\phi\phi} = \boldsymbol{I} - \hat{\boldsymbol{P}}_{\phi\phi}^{-1} \hat{\boldsymbol{K}}_{\phi\phi} \tag{118}$$

$$\boldsymbol{T}_{\phi\phi} = \boldsymbol{I} - \boldsymbol{Q} \boldsymbol{K}_{0\phi\phi}^{-1} \boldsymbol{Q}^T \boldsymbol{K}_{\phi\phi}, \qquad \hat{\boldsymbol{T}}_{\phi\phi} = \boldsymbol{I} - \tilde{\boldsymbol{Q}} \hat{\boldsymbol{K}}_{0\phi\phi}^{-1} \tilde{\boldsymbol{Q}}^T \hat{\boldsymbol{K}}_{\phi\phi} \tag{119}$$

$\boldsymbol{P}_{\phi\phi}$ and $\hat{\boldsymbol{P}}_{\phi\phi}$ are smoothing preconditioners.

5.2 Prolongation operators

5.2.1 One-dimensional case

The RVE is composed of three elements as shown in Fig. 1. Between adjacent RVEs a "soft" (with smaller stiffness) interface element is placed. For simplicity, we focus on the case of constant mass density $\rho_1 = \rho_2 = \rho$, and the volume fraction $\alpha = 0.5$.

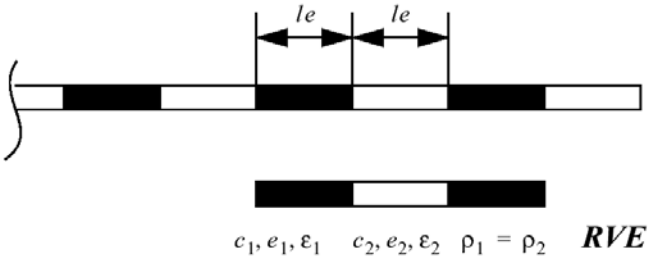

Figure 1: The 1D model with RVE

The effective dielectric and dielectric stiffness matrices of the RVE are evaluated as

$$\hat{\boldsymbol{K}}^r_{\phi\phi} = \boldsymbol{K}^r_{\phi\phi} + \frac{\Delta t^2}{4}\boldsymbol{K}^{rT}_{\boldsymbol{u}\phi}(\boldsymbol{M}^r_{\boldsymbol{uu}})^{-1}\boldsymbol{K}^r_{\boldsymbol{u}\phi} \tag{120}$$

$$\boldsymbol{K}^r_{\phi\phi} = \begin{bmatrix} a_1 & -a_1 & 0 & 0 \\ -a_1 & a_1+b_1 & -b_1 & 0 \\ 0 & -b_1 & a_1+b_1 & -a_1 \\ 0 & 0 & -a_1 & a_1 \end{bmatrix}, \quad a_1 = \varepsilon_1 A/le, \quad b_1 = \varepsilon_2 A/le \tag{121}$$

$$\boldsymbol{K}^r_{\boldsymbol{u}\phi} = \begin{bmatrix} a_2 & -a_2 & 0 & 0 \\ -a_2 & a_2+b_2 & -b_2 & 0 \\ 0 & -b_2 & a_2+b_2 & -a_2 \\ 0 & 0 & -a_2 & a_2 \end{bmatrix}, \quad a_2 = e_1 A/le, \quad b_2 = e_2 A/le \tag{122}$$

$$\boldsymbol{M}^r_{\boldsymbol{uu}} = \rho le A diag(1/2, 1, 1, 1/2) \tag{123}$$

where $\hat{\boldsymbol{K}}^r_{\phi\phi}$, $\boldsymbol{K}^r_{\phi\phi}$ and $\boldsymbol{K}^r_{\boldsymbol{u}\phi}$ are the effective dielectric, dielectric and piezoelectric stiffness matrices of the RVE, respectively; $\boldsymbol{M}^r_{\boldsymbol{uu}}$ is the lumped mass matrix of the RVE; ρ, A and le are the mass density, cross-sectional area and element length, respectively; ε_1, ε_2, e_1 and e_2 are dielectric and piezoelectric constants of the two material constituents, respectively. The prolongation operators for the RVE are constructed based on the corresponding constrained minimization problems:

$$\text{Minimize: } \Pi^1_r = \frac{1}{2}\psi_r^T \boldsymbol{K}^r_{\phi\phi}\psi_r, \quad \text{subjected to } \|\psi_r\|_2 = 1 \tag{124}$$

$$\text{Minimize: } \Pi_r^2 = \frac{1}{2}\phi_r^T \hat{\boldsymbol{K}}_{\phi\phi}^r \phi_r, \quad \text{subjected to } \|\phi_r\|_2 = 1 \tag{125}$$

which yields the following eigenvalue problems

$$\boldsymbol{K}_{\phi\phi}^r \psi_r = \mu_r \psi_r, \quad \|\psi_r\|_2 = 1 \tag{126}$$

$$\hat{\boldsymbol{K}}_{\phi\phi}^r \phi_r = \lambda_r \phi_r, \quad \|\phi_r\|_2 = 1 \tag{127}$$

The global prolongation operators $\boldsymbol{Q}$ and $\tilde{\boldsymbol{Q}}$ are block diagonal matrices:

$$\boldsymbol{Q}_{n\times m} = \text{diag}\{\boldsymbol{Q_r}, \boldsymbol{Q_r}, \ldots, \boldsymbol{Q_r}\}, \qquad \tilde{\boldsymbol{Q}}_{n\times m} = \text{diag}\{\tilde{\boldsymbol{Q}}_{\boldsymbol{r}}, \tilde{\boldsymbol{Q}}_{\boldsymbol{r}}, \ldots, \tilde{\boldsymbol{Q}}_{\boldsymbol{r}}\} \tag{128}$$

$$\boldsymbol{Q_r} = \left[\boldsymbol{p}_1\ \boldsymbol{p}_2\right], \qquad \tilde{\boldsymbol{Q}}_{\boldsymbol{r}} = \left[\boldsymbol{q}_1\ \boldsymbol{q}_2\right] \tag{129}$$

where $\boldsymbol{p}_1$ and $\boldsymbol{p}_2$ are eigenvectors corresponding to the first two smallest eigenvalues of the eigenvalue problem (126), whereas $\boldsymbol{q}_1$ and $\boldsymbol{q}_2$ are eigenvectors corresponding to the first two smallest eigenvalues of the eigenvalue problem (127).

5.2.2 Two-dimensional case

We consider a 2D structured mesh in x_1 and x_3 plane as shown in Fig.2. Plane stress assumption is made. The RVE consists 9 elements as illustrated in Fig.2. The total electric field degrees of freedom for the RVE problem is 16.

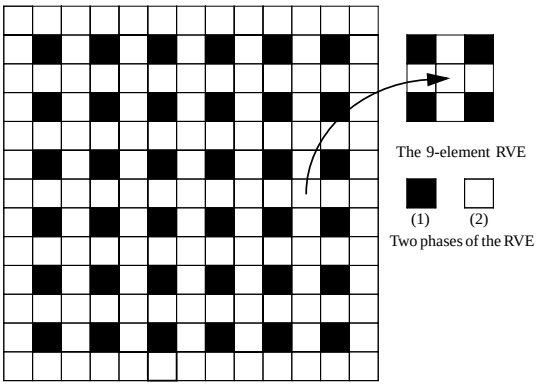

Figure 2: Global and RVE (local) finite element meshes

As in the 1D case, the global prolongation operators $\boldsymbol{Q}$ and $\tilde{\boldsymbol{Q}}$ are assembled from the prolongation matrices, $\boldsymbol{Q}_r$ and $\tilde{\boldsymbol{Q}}_r$, of RVEs. The RVE prolongation matrix consists of eigenvectors of the eigenvalue problems (126) and (127), respectively. In the numerical

examples considered, we take the first 8 eigenvectors corresponding to the lowest eigenvalues.

The two constituent phases are assumed to be made of PZT ceramic with transversely isotropic properties. The constitutive equation (3) in matrix form can be written as

$$\sigma = \boldsymbol{C}\boldsymbol{S} - \boldsymbol{e}^T\boldsymbol{E}, \qquad \boldsymbol{D} = \boldsymbol{e}\boldsymbol{S} + \varepsilon\boldsymbol{E} \tag{130}$$

where

$$\sigma = \left[\sigma_1\ \sigma_2\ \sigma_3\ \sigma_4\ \sigma_5\ \sigma_6\right]^T, \qquad \boldsymbol{S} = \left[S_1\ S_2\ S_3\ S_4\ S_5\ S_6\right]^T \tag{131}$$

$$\boldsymbol{D} = \left[D_1\ D_2\ D_3\right]^T, \qquad \boldsymbol{E} = \left[E_1\ E_2\ E_3\right]^T \tag{132}$$

$$\boldsymbol{C}_{\lambda\mu} = \begin{bmatrix} c_{11} & c_{12} & c_{13} & 0 & 0 & 0 \\ c_{12} & c_{11} & c_{13} & 0 & 0 & 0 \\ c_{13} & c_{13} & c_{33} & 0 & 0 & 0 \\ 0 & 0 & 0 & c_{44} & 0 & 0 \\ 0 & 0 & 0 & 0 & c_{44} & 0 \\ 0 & 0 & 0 & 0 & 0 & (c_{11}-c_{12})/2 \end{bmatrix}, \qquad \varepsilon_{ij} = \begin{bmatrix} \varepsilon_{11} & 0 & 0 \\ 0 & \varepsilon_{11} & 0 \\ 0 & 0 & \varepsilon_{33} \end{bmatrix}$$

$$\boldsymbol{e}_{i\lambda} = \begin{bmatrix} 0 & 0 & 0 & 0 & e_{15} & 0 \\ 0 & 0 & 0 & e_{15} & 0 & 0 \\ e_{31} & e_{31} & e_{33} & 0 & 0 & 0 \end{bmatrix}, \quad \lambda, \mu = 1, 2, \ldots, 6; \quad i, j = 1, 2, 3 \tag{133}$$

Tensor and matrix indices are related by

$$11 \to 1,\ 22 \to 2,\ 33 \to 3,\ 23 \to 4,\ 31 \to 5,\ 12 \to 6$$

or alternatively

$$\lambda = \frac{1}{2}(i+j)\delta_{ij} + [9-(i+j)](1-\delta_{ij})$$

where δ_{ij} is the Kronecker delta. Components of stress and strain tensors and matrices are related as

Stress: $\sigma_{ij} \to \sigma_\lambda$

Strain: $S_{ij} \to S_\lambda$ for $i = j$ $(\lambda = 1, 2, 3)$; $2S_{ij} \to S_\lambda$ for $i \neq j$ $(\lambda = 4, 5, 6)$

For plane stress in x_1 and x_3 plane $\sigma_2 = \sigma_4 = \sigma_6 = 0$ and $E_2 = 0$.

The constitutive equation (130) in the matrix form can be simplified as

$$\begin{bmatrix} \sigma_1 \\ \sigma_3 \\ \sigma_5 \end{bmatrix} = \begin{bmatrix} \tilde{c}_{11} & \tilde{c}_{13} & 0 \\ \tilde{c}_{13} & \tilde{c}_{33} & 0 \\ 0 & 0 & c_{44} \end{bmatrix} \begin{bmatrix} S_1 \\ S_3 \\ S_5 \end{bmatrix} - \begin{bmatrix} 0 & \tilde{e}_{31} \\ 0 & \tilde{e}_{33} \\ e_{15} & 0 \end{bmatrix} \begin{bmatrix} E_1 \\ E_3 \end{bmatrix} \tag{134}$$

$$\begin{bmatrix} D_1 \\ D_3 \end{bmatrix} = \begin{bmatrix} 0 & 0 & e_{15} \\ \tilde{e}_{31} & \tilde{e}_{33} & 0 \end{bmatrix} \begin{bmatrix} S_1 \\ S_3 \\ S_5 \end{bmatrix} + \begin{bmatrix} \varepsilon_{11} & 0 \\ 0 & \tilde{\varepsilon}_{33} \end{bmatrix} \begin{bmatrix} E_1 \\ E_3 \end{bmatrix} \tag{135}$$

where

$$\tilde{c}_{11} = c_{11} - c_{12}^2/c_{11}, \quad \tilde{c}_{13} = c_{13} - c_{12}c_{13}/c_{11}, \quad \tilde{c}_{33} = c_{33} - c_{13}^2/c_{11}$$

$$\tilde{e}_{31} = e_{31} - e_{31}c_{12}/c_{11}, \quad \tilde{e}_{33} = e_{33} - e_{31}c_{13}/c_{11}, \quad \tilde{\varepsilon}_{33} = \varepsilon_{33} + e_{31}^2/c_{11} \tag{136}$$

The spectral radii of the two-level iteration matrices $\rho(\boldsymbol{L}_{\phi\phi})$ and $\rho(\hat{\boldsymbol{L}}_{\phi\phi})$ with $\upsilon = 3$ are evaluated numerically and the results are presented in Table 1 through Table 4, in which n is the size of the source mesh and $\Delta t_{cr} = 2/\omega_n^{im}$ is the critical time step for the implicit conditionally stable partitioned scheme; $\tilde{\varepsilon}_{11} = \varepsilon_{11}$, $\tilde{c}_{44} = c_{44}$ and $\tilde{e}_{15} = e_{15}$.

For the explicit and implicit conditionally stable partitioned schemes, the coefficient matrix of the electric field equation is simply the dielectric stiffness matrix. It only depends on the dielectric constants of the media. From Table 1 and Table 2, it can be observed that the rate of convergence improves with increasing heterogeneity in dielectric constants and is independent of the problem size.

TABLE 1. Spectral radius of the 1D two-level iteration matrix $\rho(\boldsymbol{L}_{\phi\phi})$

$\rho(\boldsymbol{S}_{\phi\phi}^3 \boldsymbol{T}_{\phi\phi} \boldsymbol{S}_{\phi\phi}^3)$	$n = 100$	$n = 200$	$n = 300$
$\varepsilon_1/\varepsilon_2 = 1$	0.0243	0.0243	0.0243
$\varepsilon_1/\varepsilon_2 = 50$	0.0206	0.0206	0.0206
$\varepsilon_1/\varepsilon_2 = 100$	0.0116	0.0116	0.0116
$\varepsilon_1/\varepsilon_2 = 1000$	0.0013	0.0013	0.0013

TABLE 2. Spectral radius of the 2D two-level iteration matrix $\rho(\boldsymbol{L}_{\phi\phi})$

$\rho(\boldsymbol{S}^3_{\phi\phi}\boldsymbol{T}_{\phi\phi}\boldsymbol{S}^3_{\phi\phi})$	$n = 14 \times 14$	$n = 22 \times 22$	$n = 30 \times 30$
$\tilde{\varepsilon}^{(1)}_{ii}/\tilde{\varepsilon}^{(2)}_{ii} = 1$	0.0216	0.0356	0.0420
$\tilde{\varepsilon}^{(1)}_{ii}/\tilde{\varepsilon}^{(2)}_{ii} = 50$	0.0204	0.0212	0.0214
$\tilde{\varepsilon}^{(1)}_{ii}/\tilde{\varepsilon}^{(2)}_{ii} = 100$	0.0136	0.0138	0.0139
$\tilde{\varepsilon}^{(1)}_{ii}/\tilde{\varepsilon}^{(2)}_{ii} = 1000$	0.0020	0.0021	0.0021

The coefficient matrix of the unconditionally stable partitioned scheme is the effective dielectric matrix, which depends on the time step, the dielectric and piezoelectric constants. From Table 3 and Table 4, we can observe that the rate of convergence improves with increasing heterogeneity in dielectric constants, but increasing heterogeneity in piezoelectric constants tends to affect the rate of convergence adversely. In all cases, the rate of convergence improves with decreasing time step and is independent of the problem size.

TABLE 3. Spectral radius of the 1D two-level iteration matrix $\rho(\hat{\boldsymbol{L}}_{\phi\phi})$

	$n = 100$		$n = 200$	
$\rho(\hat{\boldsymbol{S}}^3_{\phi\phi}\hat{\boldsymbol{T}}_{\phi\phi}\hat{\boldsymbol{S}}^3_{\phi\phi})$	$\Delta t/\Delta t_{cr} = 1$	$\Delta t/\Delta t_{cr} = 10$	$\Delta t/\Delta t_{cr} = 1$	$\Delta t/\Delta t_{cr} = 10$
$e_1/e_2 = 1, \varepsilon_1/\varepsilon_2 = 1$	0.0767	0.8558	0.0767	0.8569
$e_1/e_2 = 1, \varepsilon_1/\varepsilon_2 = 100$	0.0301	0.2846	0.0302	0.2846
$e_1/e_2 = 1, \varepsilon_1/\varepsilon_2 = 1000$	0.0039	0.1170	0.0039	0.1170
$e_1/e_2 = 4, \varepsilon_1/\varepsilon_2 = 1$	0.0783	0.6484	0.0784	0.6485
$e_1/e_2 = 4, \varepsilon_1/\varepsilon_2 = 100$	0.0638	0.8378	0.0639	0.8380
$e_1/e_2 = 4, \varepsilon_1/\varepsilon_2 = 1000$	0.0102	0.4262	0.0102	0.4262
$e_1/e_2 = 10, \varepsilon_1/\varepsilon_2 = 1$	0.9976	0.9999	0.9994	1.0000
$e_1/e_2 = 10, \varepsilon_1/\varepsilon_2 = 100$	0.0871	0.9185	0.0871	0.9187

TABLE 4. Spectral radius of the 2D two-level iteration matrix $\rho(\hat{\boldsymbol{L}}_{\phi\phi})$

	$n = 22 \times 22$		$n = 30 \times 30$	
$\rho(\hat{\boldsymbol{S}}^3_{\phi\phi}\hat{\boldsymbol{T}}_{\phi\phi}\hat{\boldsymbol{S}}^3_{\phi\phi})$	$\Delta t/\Delta t_{cr} = 1$	$\Delta t/\Delta t_{cr} = 10$	$\Delta t/\Delta t_{cr} = 1$	$\Delta t/\Delta t_{cr} = 10$
$r_1 = 1, r_2 = 1$	0.0726	0.4414	0.0808	0.4901
$r_1 = 1, r_2 = 100$	0.0360	0.2121	0.0366	0.2254
$r_1 = 1, r_2 = 1000$	0.0055	0.1322	0.0056	0.1386
$r_1 = 10, r_2 = 1$	0.0659	0.5116	0.0749	0.5621
$r_1 = 10, r_2 = 100$	0.0963	0.7231	0.0983	0.7872
$r_1 = 10, r_2 = 1000$	0.0249	0.6088	0.0252	0.6598
$r_1 = 100, r_2 = 1$	0.1073	0.0386	0.1290	0.0416
$r_1 = 100, r_2 = 100$	0.0187	0.9997	0.0195	0.9999
$r_1 = 100, r_2 = 1000$	0.0386	0.9999	0.0402	1.0000

$r_1 = \tilde{e}^{(1)}_{i\lambda}/\tilde{e}^{(2)}_{i\lambda}$, $\quad r_2 = \tilde{\varepsilon}^{(1)}_{ii}/\tilde{\varepsilon}^{(2)}_{ii}$

To this end we compare the critical time steps of the implicit conditionally stable and the explicit partitioned schemes in 2D case. Numerical results reveal that the ratio of critical time steps in implicit and explicit schemes is only slightly affected by the heterogeneity in dielectric and piezoelectric constants, but is extremely sensitive to the heterogeneity in elastic constants. In Fig. 3, we plot the ratio of critical time steps between the implicit and explicit schemes as well as the spectral radius of the two-level iteration matrix for the mechanical equation versus the ratio of elastic constants $\tilde{c}_{\lambda\mu}^{(1)}/\tilde{c}_{\lambda\mu}^{(2)}$.

It can be observed from Fig. 3 that with increasing ratio of elastic constants of the two constituent phases, the spectral radius of the two-level iteration matrix for the mechanical equation decreases and the ratio of critical time steps increases. Thus the implicit conditionally stable partitioned scheme can use a larger time step than that used for the explicit scheme at the expense of solving a linear system of mechanical equations at each time station. When the mismatch of mechanical properties is considerable, the spectral radius of the two-level iteration matrix for the mechanical equation could be sufficiently small for the two-level iteration process to converge in a couple of cycles.

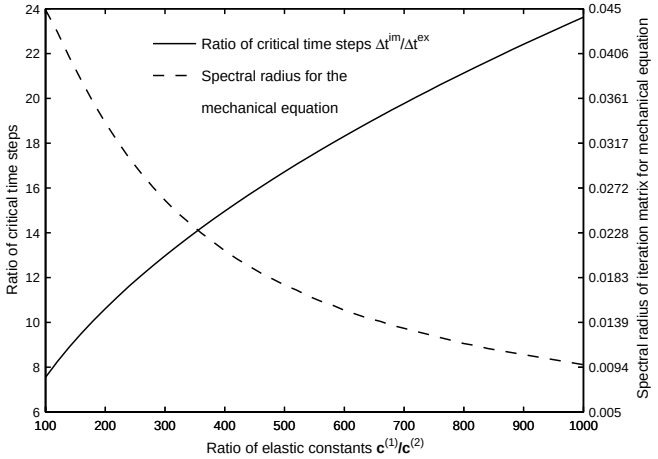

Figure 3. Ratio of critical time steps and spectral radius of mechanical equation versus the ratio of elastic constants.

5.3 Convergence of the two-level method

Consider the problem illustrated in Fig.1. The bar is fixed at ($x = 0$) and free at ($x = 1$) with no external load and electric charge acting on the bar. The following initial disturbance in the displacement field is considered:

$$f(x) = f_0 a_0 [x-(x_0-\delta)]^4 [x-(x_0+\delta)]^4 \{1-H[x-(x_0+\delta)]\}[1-H(x_0-\delta-x)]$$

where $a_0 = 1/\delta^8$ and $H(x)$ is the Heaviside step function; f_0, x_0 and δ are the magnitude, the location of the maximum value and the half width of the initial pulse. This pulse is similar in shape to the Gaussian distribution function. In the computations, we take $x_0 = 1/2$ and $f_0 = 0.05$.

For both electric and mechanical equations, we employ three SSOR pre- and post-smoothing iterations. The stopping criterion is taken as

$$\frac{\|\boldsymbol{r}\|_2}{\|\boldsymbol{f}\|_2} \leq Tol = 10^{-6} \tag{137}$$

where $\|\boldsymbol{r}\|_2$ and $\|\boldsymbol{f}\|_2$ are the 2-norms of the residual and the right-hand-side vectors, respectively.

For parametric study of convergence characteristics of the RVE-based multilevel solver, we carry out computations with different ratios of material constants. The results are summarized in Table 5 and Table 6 for the implicit conditionally and unconditionally stable partitioned schemes, respectively. In both tables, the numbers in the parentheses correspond to the cycle count of the mechanical equation, while the numbers without parentheses denote the cycle numbers for the electric field equation. For the conditionally stable scheme, we take $\Delta t = \Delta t_{cr}^{im}$.

TABLE 5. Numbers of cycles for the conditionally stable scheme ($Tol = 10^{-6}$)

Iteration Numbers	$n = 400$	$n = 1000$	$n = 2000$
$c_1/c_2 = 1, e_1/e_2 = 1, \varepsilon_1/\varepsilon_2 = 1$	4(2)	4(2)	4(2)
$c_1/c_2 = 1, e_1/e_2 = 1, \varepsilon_1/\varepsilon_2 = 10$	4(2)	4(2)	4(2)
$c_1/c_2 = 1, e_1/e_2 = 1, \varepsilon_1/\varepsilon_2 = 100$	3(2)	3(2)	3(2)
$c_1/c_2 = 1, e_1/e_2 = 1, \varepsilon_1/\varepsilon_2 = 1000$	2(2)	2(2)	2(2)
$c_1/c_2 = 1, e_1/e_2 = 4, \varepsilon_1/\varepsilon_2 = 100$	3(2)	3(2)	3(2)
$c_1/c_2 = 10, e_1/e_2 = 2, \varepsilon_1/\varepsilon_2 = 2$	4(4)	3(3)	3(3)
$c_1/c_2 = 100, e_1/e_2 = 2, \varepsilon_1/\varepsilon_2 = 2$	4(3)	3(3)	3(3)
$c_1/c_2 = 1000, e_1/e_2 = 2, \varepsilon_1/\varepsilon_2 = 2$	4(2)	3(2)	3(2)

TABLE 6. Numbers of cycles for the unconditionally stable scheme ($Tol = 10^{-6}$)

Iteration Numbers	$n = 400$		$n = 1000$	
	$\Delta t/\Delta t_{cr} = 1$	$\Delta t/\Delta t_{cr} = 10$	$\Delta t/\Delta t_{cr} = 1$	$\Delta t/\Delta t_{cr} = 10$
$c_1/c_2 = 1, e_1/e_2 = 1, \varepsilon_1/\varepsilon_2 = 1$	6(2)	64(4)	5(2)	87(4)
$c_1/c_2 = 1, e_1/e_2 = 1, \varepsilon_1/\varepsilon_2 = 10$	5(2)	26(4)	5(2)	29(4)
$c_1/c_2 = 1, e_1/e_2 = 1, \varepsilon_1/\varepsilon_2 = 100$	4(2)	9(4)	4(2)	9(4)
$c_1/c_2 = 1, e_1/e_2 = 1, \varepsilon_1/\varepsilon_2 = 1000$	3(2)	6(4)	3(2)	6(4)
$c_1/c_2 = 1, e_1/e_2 = 4, \varepsilon_1/\varepsilon_2 = 100$	5(2)	55(4)	5(2)	65(4)
$c_1/c_2 = 10, e_1/e_2 = 2, \varepsilon_1/\varepsilon_2 = 2$	4(4)	37(4)	4(3)	37(4)
$c_1/c_2 = 100, e_1/e_2 = 2, \varepsilon_1/\varepsilon_2 = 2$	4(4)	37(3)	4(3)	36(3)
$c_1/c_2 = 1000, e_1/e_2 = 2, \varepsilon_1/\varepsilon_2 = 2$	4(3)	35(2)	4(2)	35(2)

From Table 5 and Table 6, it can be seen that the RVE-based multilevel method converges faster for the mechanical equation than for the electric equation. Moreover, increasing the ratios of elastic and dielectric constants, and cutting the time step size tend to reduce the number of cycles.

Acknowledgment

The support of the Sandia National Laboratories under Contract DE-AL04-94AL8500 and the Office of Naval Research through grant number N00014-97-1-0687 are gratefully acknowledged.

References

1 Felippa CA., Park KC. and Farhat C., Partitioned analysis of coupled mechanical systems. *Comput. Methods Appl. Mech. Engrg.*, **190**:3247-3270, 2001.

2 Piperno S. and Farhat C., Partitioned procedures for the transient solution of coupled aeroelastic problems, Part II: energy transfer analysis and three-dimensional applications. *Comput. Methods Appl. Mech. Engrg.*, **190**: 3147-3170, 2001.

3 E.Tursa and B.A.Schrefler, "On consistency, stability and convergence of staggered solution procedures,"Rend. Mat. acc. Lincei, Rome, S. 9, v.5, pp. 265-271, 1994.

4 Fish J. and Belsky V., Multigrid method for a periodic heterogeneous medium. Part I: Convergence studies for one-dimensional case. *Comp. Meth. Appl. Mech. Engng*., **126:** 1-16, 1995.

5 Fish J. and Belsky V., Multigrid method for a periodic heterogeneous medium. Part 2: Multiscale modeling and quality control in multidimensional case. *Comp. Meth. Appl. Mech. Engng*., **126:** 17-38, 1995.

6 Fish J. and Chen W., RVE based multilevel method for periodic heterogeneous media with strong scale mixing, submitted to *Journal of Applied Mathematics*, 2002.

7 Tiersten HF., *Linear Piezoelectric Plate Vibrations, Elements of the Linear Theory of Piezoelectricity and the Vibrations of Piezoelectric Plates*. Plenum Press: New York, 1967.

8 Lim YH., Varadan VV. and Varadan VK., Finite-element modeling of the transient response of MEMS sensors. *Smart Mater. Struct.*, **6:** 53-61, 1997.

9 Chen CQ., Wang XM. and Shen YP., Finite element approach of vibration control using self-sensing piezoelectric actuators. *Computers & Structures*, **60(3):** 505-512, 1996.

10 Kagawa Y., Tsuchiya T. and Kataoka T., Finite element simulation of dynamic responses of piezoelectric actuators. *Journal of Sound and Vibration*, **191(4):** 519-538, 1996.

11 Saravanos DA., Heyliger PR. and Hopkins DA., Layerwise mechanics and finite element for the dynamic analysis of piezoelectric composite plates. *Int. J. Solids Struc-*

tures, **34(3):** 359-378, 1997.

12 Aldraihem OJ. and Wetherhold RC., Mechanics and control of coupled bending and twisting vibration of laminated beams. *Smart Mater. Struct.*, **6:** 123-133, 1997.

13 Hughes TJR., *The Finite Element Method, Linear Static and Dynamic Finite Element Analysis*. Prentice-Hall: Englewood Cliffs. NJ, 1987.

14 Hughes TJR., Analysis of transient algorithms with particular reference to stability behavior. In: *Computational Methods For Transient Analysis*, Belytschko T. and Hughes TJR. (eds.), North-Holland: Amsterdam, New York, Oxford, 1983.

15 Farhat C., Park KC. and Pelerin YD., An unconditionally stable staggered algorithm for transient finite element analysis of coupled thermoelastic problems. *Comput. Methods Appl. Mech. Engrg.*, **85**: 349-365, 1991.

16 Zienkiewicz OC., Paul DK. and Chan AHC., Unconditionally stable staggered solution procedure for soil-pore fluid interaction problems. *Int. J. Numer. Meth. Engng.,* **26:** 1039-1055, 1988.

17 Lambert JD., *Computational Methods in Ordinary Differential Equations*. Wiley: London, 1973.

18 Bellman R., *Introduction to Matrix Analysis*. McGraw-Hill Inc., New York, 1960.

19 Fish J. and Qu Y., Global basis two-level method for indefinite systems. Part 1: convergence studies. *Int. J. Numer. Meth. Engng.,* **49:** 439-460, 2000.

20 Qu Y. and Fish J., Global basis two-level method for indefinite systems. Part 2: Computational issues. *Int. J. Numer. Meth. Engng.,* **49:** 461-478, 2000.

21 Challande P., Optimizing ultrasonic transducers based on piezoelectric composites using a finite element method. *IEEE Transactions on Ultrasonics, Ferroelectrics and Frequency Control*, **37(2):** 135-140, 1990.

22 Lerch R., Simulation of piezoelectric devices by two- and three-dimensional finite elements. *IEEE Transactions on Ultrasonics, Ferroelectrics and Frequency Control*, **37(2):** 233-247, 1990.

23 Abboud NN., Wojcik GL., Vaughan DK., Mould J., Powell DJ., and Nikodym L., Finite element modeling of ultrasonic transducers. *Proc. SPIE Int. Symp. Medical Imaging,* San Diego, Feb 21-27, 1998.